

New LUX and PandaX-II Results Illuminating the Simplest Higgs-Portal Dark Matter Models

Xiao-Gang He^{1,2,3*} and Jusak Tandean^{2,3†}

¹*INPAC, Department of Physics and Astronomy, Shanghai Jiao Tong University,
800 Dongchuan Rd., Minhang, Shanghai 200240, China*

²*Department of Physics and Center for Theoretical Sciences, National Taiwan University,
No. 1, Sec. 4, Roosevelt Rd., Taipei 106, Taiwan*

³*Physics Division, National Center for Theoretical Sciences,
No. 101, Sec. 2, Kuang Fu Rd., Hsinchu 300, Taiwan*

Abstract

Direct searches for dark matter (DM) by the LUX and PandaX-II Collaborations employing xenon-based detectors have recently come up with the most stringent limits to date on the spin-independent elastic scattering of DM off nucleons. For Higgs-portal scalar DM models, the new results have precluded any possibility of accommodating low-mass DM as suggested by the DAMA and CDMS II Si experiments utilizing other target materials, even after invoking isospin-violating DM interactions with nucleons. In the simplest model, SM+D, which is the standard model plus a real singlet scalar named darkon acting as the DM candidate, the LUX and PandaX-II limits rule out DM masses roughly from 4 to 450 GeV, except a small range around the resonance point at half of the Higgs mass where the interaction cross-section is near the neutrino-background floor. In the THDM II+D, which is the type-II two-Higgs-doublet model combined with a darkon, the region excluded in the SM+D by the direct searches can be recovered due to suppression of the DM effective interactions with nucleons at some values of the ratios of Higgs couplings to the up and down quarks, making the interactions significantly isospin-violating. However, in either model, if the 125-GeV Higgs boson is the portal between the dark and SM sectors, DM masses less than 50 GeV or so are already ruled out by the LHC constraint on the Higgs invisible decay. In the THDM II+D, if the heavier CP -even Higgs boson is the portal, theoretical restrictions from perturbativity, vacuum stability, and unitarity requirements turn out to be important instead and exclude much of the region below 100 GeV. For larger DM masses, the THDM II+D has plentiful parameter space that corresponds to interaction cross-sections under the neutrino-background floor and therefore is likely to be beyond the reach of future direct searches without directional sensitivity.

*Electronic address: hexg@phys.ntu.edu.tw

†Electronic address: jtandean@yahoo.com

I. INTRODUCTION

Cosmological studies have led to the inference that ordinary matter makes up only about 5% of the energy budget of the Universe, the rest being due to dark matter (26%) and dark energy (69%), the properties of which are largely still unknown [1]. Although the evidence for cosmic dark matter (DM) has been established for decades from numerous observations of its gravitational effects, the identity of its basic constituents has so far remained elusive. As the standard model (SM) of particle physics cannot account for the bulk of the DM, it is of great interest to explore various possible scenarios beyond the SM that can accommodate it. Amongst the multitudes of DM candidates that have been proposed in the literature, those classified as weakly interacting massive particles (WIMPs) are perhaps the leading favorites [1]. The detection of a WIMP is then essential not only for understanding the nature of the DM particle, but also for distinguishing models of new physics beyond the SM.

Many different underground experiments have been and are being performed to detect WIMPs directly by looking for the signatures of nuclear recoils caused by the collisions between the DM and nucleons. The majority of these searches have so far come up empty, leading only to upper bounds on the cross section σ_{el}^N of spin-independent elastic WIMP-nucleon scattering. Experiments utilizing xenon as the target material have turned out to supply the strictest bounds to date, especially the newest ones reported separately by the LUX and PandaX-II Collaborations [2, 3], under the implicit assumption that the DM interactions with the proton and neutron respect isospin symmetry. These null results are in conflict with the tentative indications of WIMP signals observed earlier at relatively low masses in the DAMA [4] and CDMS II Si [5] measurements, which employed nonxenon target materials.¹ A graphical comparison between the new limits on σ_{el}^N from LUX and PandaX-II and the hypothetical signal regions suggested by DAMA and CDMS II Si is presented in Fig. 1(a). It also displays the limits from a few other direct searches [9–11], which were more sensitive to lighter WIMPs, as well as the expected reaches [12] of the upcoming XENON1T [13], DarkSide G2 [14], and LZ [15] experiments and an estimate of the WIMP discovery limit due to coherent neutrino scattering backgrounds [16].

Mechanisms that may reconcile the incompatible null and positive results of the WIMP DM direct searches have been suggested over the years. One of the most appealing proposals stems from the realization that the effective couplings f_p and f_n of the DM to the proton and neutron, respectively, may be very dissimilar [17, 18]. If such a substantial violation of isospin symmetry occurs, the impact on the detection sensitivity to WIMP collisions can vary significantly, depending on the target material. In particular, during the collision process the DM may manifest a xenophobic behavior brought about by severe suppression of the collective coupling of the DM to xenon nuclei, but not necessarily to other nuclei [19]. This can explain why xenon-based detectors still have not discovered any DM, but DAMA and CDMS II Si perhaps did. Numerically, in the xenon case the suppression is the strongest if $f_n/f_p \simeq -0.7$ [18]. Assuming this ratio and applying it to the pertinent formulas provided in Ref. [18], one can translate the data in Fig. 1(a) into the corresponding numbers for the spin-independent elastic WIMP-proton cross-section, σ_{el}^p .

¹ The excess events previously observed in the CoGeNT [6] and CRESST-II [7] experiments have recently been demonstrated to be entirely attributable to underestimated backgrounds instead of DM recoils [8].

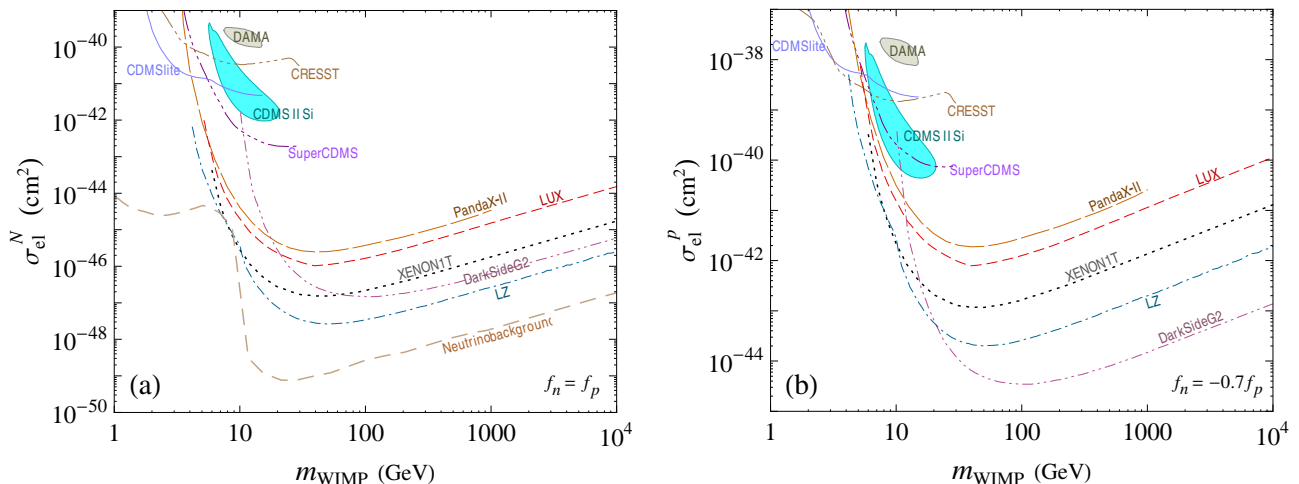


FIG. 1: (a) Measured upper-limits on the spin-independent elastic WIMP-nucleon cross-section at 90% confidence level (CL) versus WIMP mass from LUX [2], PandaX-II [3], CDMSlite [9], SuperCDMS [10], and CRESST [11] in the isospin-symmetric limit. Also shown are a gray patch compatible with the DAMA Na modulation signal at the 3σ level [20], a cyan area for the possible DM hint from CDMS II Si at 90% CL [5], the sensitivity projections [12] of XENON1T [13] (black dotted curve), DarkSide G2 [14] (maroon dash-dot-dotted curve), and LZ [15] (turquoise dash-dotted curve), and the WIMP discovery lower-limit due to coherent neutrino scattering backgrounds [16] (brown dashed curve). (b) The corresponding WIMP-proton cross-sections computed from (a) with isospin-violating effective WIMP couplings to the neutron and proton in the ratio $f_n/f_p = -0.7$.

The latter are plotted in Fig. 1(b), where the curve for DarkSide G2, which will employ an argon target, is scaled up differently from the curves for the xenon experiments including LZ. It is now evident that the conjectured signal regions of DAMA and CDMS II Si are no longer viable in light of the latest LUX and PandaX-II bounds.²

Since these new results have reduced further the allowed WIMP parameter space, it is of interest to investigate what implications they may have for the simplest Higgs-portal WIMP DM models and how these scenarios may be probed more stringently in the future. For definiteness, in this paper we focus on the SM+D, which is the SM minimally expanded with the addition of a real singlet scalar serving as the DM and dubbed darkon, and on its two-Higgs-doublet extension of type II, which we call THDMII+D.³ Specifically, we look at a number of constraints on these two models not only from the most recent DM direct searches, but also from LHC measurements on the gauge and Yukawa couplings of the 125-GeV Higgs boson and on its invisible decay mode, as

² If the DM-nucleon scattering is both isospin violating and inelastic, which can happen if a spin-1 particle, such as a Z' boson, is the portal between the DM and SM particles, it may still be possible to accommodate the potential hint of low-mass DM from CDMS II Si and evade the limits from xenon detectors at the same time [21]. The inelastic-DM approach has also been proposed to explain the DAMA anomaly [22].

³ There are earlier studies in the literature on various aspects of the SM plus singlet scalar DM, or a greater scenario containing the model, in which the scalar was real [23–25] or complex [26]. Two-Higgs-doublet extensions of the SM+D have also been explored previously [27–31].

well as from some theoretical requirements. We find that in the SM+D the darkon mass region up to ~ 450 GeV is ruled out, except a small range near the resonant point at half of the Higgs mass where the DM-nucleon cross-section is close to the neutrino-background floor. On the other hand, in the THDMII+D the region excluded in the SM+D can be partially recovered because of suppression of the cross section that happens at some values of the product $\tan\alpha \tan\beta$ or $\cot\alpha \tan\beta$, where α is the mixing angle of the CP -even Higgs bosons and $\tan\beta$ the ratio of vacuum expectation values (VEVs) of the Higgs doublets.

The structure of the rest of the paper is as follows. We treat the SM+D in Sec. II and the THDMII+D in Sec. III. We summarize our results and conclude in Sec. IV. A couple of appendices contain additional formulas and extra details.

II. CONSTRAINTS ON SM+D

The darkon, D , in the SM+D is a real scalar field and transforms as a singlet under the gauge group of the SM. Being the DM candidate, D is stable due to an exactly conserved discrete symmetry, Z_2 , under which $D \rightarrow -D$, all the other fields being unaffected. The renormalizable darkon Lagrangian then has the form [23]

$$\mathcal{L}_D = \frac{1}{2} \partial^\mu D \partial_\mu D - \frac{1}{4} \lambda_D D^4 - \frac{1}{2} m_0^2 D^2 - \lambda D^2 H^\dagger H, \quad (1)$$

where λ_D , m_0 , and λ are free parameters and H is the Higgs doublet containing the physical Higgs field h . After electroweak symmetry breaking

$$\mathcal{L}_D \supset -\frac{\lambda_D}{4} D^4 - \frac{(m_0^2 + \lambda v^2)}{2} D^2 - \frac{\lambda}{2} D^2 h^2 - \lambda D^2 h v, \quad (2)$$

where the second term contains the darkon mass $m_D = (m_0^2 + \lambda v^2)^{1/2}$, the last two terms play an important role in determining the DM relic density, and $v \simeq 246$ GeV is the vacuum expectation value (VEV) of H . Clearly, the darkon interactions depend on a small number of free parameters, the relevant ones here being the darkon-Higgs coupling λ , which pertains to the relic density, and the darkon mass m_D .

In the SM+D, the relic density results from the annihilation of a darkon pair into SM particles which is induced mainly by the Higgs-exchange process $DD \rightarrow h^* \rightarrow X_{\text{SM}}$, where X_{SM} includes all kinematically allowed final states at the darkon pair's center-of-mass (c.m.) energy, \sqrt{s} . If the energy exceeds twice the Higgs mass, $\sqrt{s} > 2m_h$, the channel $DD \rightarrow hh$ also contributes, which arises from contact and (s, t, u)-channel diagrams. Thus, we can write the cross section σ_{ann} of the darkon annihilation into SM particles as

$$\begin{aligned} \sigma_{\text{ann}} &= \sigma(DD \rightarrow h^* \rightarrow X_{\text{SM}}) + \sigma(DD \rightarrow hh), \\ \sigma(DD \rightarrow h^* \rightarrow X_{\text{SM}}) &= \frac{4\lambda^2 v^2}{(m_h^2 - s)^2 + \Gamma_h^2 m_h^2} \frac{\sum_i \Gamma(\tilde{h} \rightarrow X_{i,\text{SM}})}{\sqrt{s - 4m_D^2}}, \quad X_{\text{SM}} \neq hh, \end{aligned} \quad (3)$$

with \tilde{h} being a virtual Higgs having the same couplings as the physical h and an invariant mass equal to \sqrt{s} , and the expression for $\sigma(DD \rightarrow hh)$ can be found in Appendix A, which also

includes an outline of how λ is extracted from the observed abundance of DM. The resulting values of λ can then be tested with constraints from other experimental information.

In numerical work, we take $m_h = 125.1$ GeV, based on the current data [32], and correspondingly the SM Higgs width $\Gamma_h^{\text{SM}} = 4.08$ MeV [33]. For $m_D < m_h/2$, the invisible decay channel $h \rightarrow DD$ is open and contributes to the Higgs' total width $\Gamma_h = \Gamma_h^{\text{SM}} + \Gamma(h \rightarrow DD)$ in Eq. (3), where

$$\Gamma(h \rightarrow DD) = \frac{\lambda^2 v^2}{8\pi m_h} \sqrt{1 - \frac{4m_D^2}{m_h^2}}. \quad (4)$$

The Higgs measurements at the LHC provide information pertinent to this process. In the latest combined analysis on their Higgs data, the ATLAS and CMS Collaborations [34] have determined the branching fraction of h decay into channels beyond the SM to be $\mathcal{B}_{\text{BSM}}^{\text{exp}} = 0.00^{+0.16}$, which can be interpreted as setting a cap on the Higgs invisible decay, $\mathcal{B}(h \rightarrow \text{invisible})_{\text{exp}} < 0.16$. Accordingly, we can impose

$$\mathcal{B}(h \rightarrow DD) = \frac{\Gamma(h \rightarrow DD)}{\Gamma_h} < 0.16, \quad (5)$$

which as we will see shortly leads to a major restriction on λ for $m_D < m_h/2$.

Direct searches for DM look for the nuclear recoil effects of DM scattering off a nucleon, N . In the SM+D, this is an elastic reaction, $DN \rightarrow DN$, which is mediated by the Higgs in the t channel and has a cross section of

$$\sigma_{\text{el}}^N = \frac{\lambda^2 g_{NNh}^2 m_N^2 v^2}{\pi (m_D + m_N)^2 m_h^4} \quad (6)$$

for momentum transfers small relative to m_h , where g_{NNh} is the Higgs-nucleon effective coupling. Numerically, we adopt $g_{NNh} = 0.0011$, which lies at the low end of our earlier estimates [28, 35] and is comparable to other recent calculations [25, 36]. The strictest limitations on σ_{el}^N to date are supplied by the newest null findings of LUX [2] and PandaX-II [3].

To show how these data confront the SM+D, we display in Fig. 2(a) the values of $|\lambda|$ derived from the observed relic abundance (green solid curve) and compare them to the upper bounds on $|\lambda|$ inferred from Eq. (5) based on the LHC information on the Higgs invisible decay [34] (black dotted curve) and from the new results of LUX [2] (red dashed curve) and PandaX-II [3] (orange dashed curve). The plot in Fig. 2(b) depicts the corresponding prediction for σ_{el}^N (green curve) in comparison to the same DM direct search data and future potential limits as in Fig. 1(a).

In the SM+D context, the graphs in Fig. 2 reveal that the existing data rule out darkon masses below about 450 GeV, except for the narrow dip area in the neighborhood of $m_D = m_h/2$, more precisely $52.1 \text{ GeV} \lesssim m_D \lesssim 62.6 \text{ GeV}$. At $m_D = m_h/2$, the threshold point for $h \rightarrow DD$, the darkon annihilation into SM particles undergoes a resonant enhancement, and consequently a small size of λ can lead to the correct relic density and, at the same time, a low cross-section of darkon-nucleon collision. However, as Fig. 2 indicates, the bottom of the λ dip does not go to zero due to the Higgs' finite total width Γ_h and the annihilation cross-section at the resonant point being proportional to $1/\Gamma_h^2$. It is interesting to note that in Fig. 2(b) the bottom of the

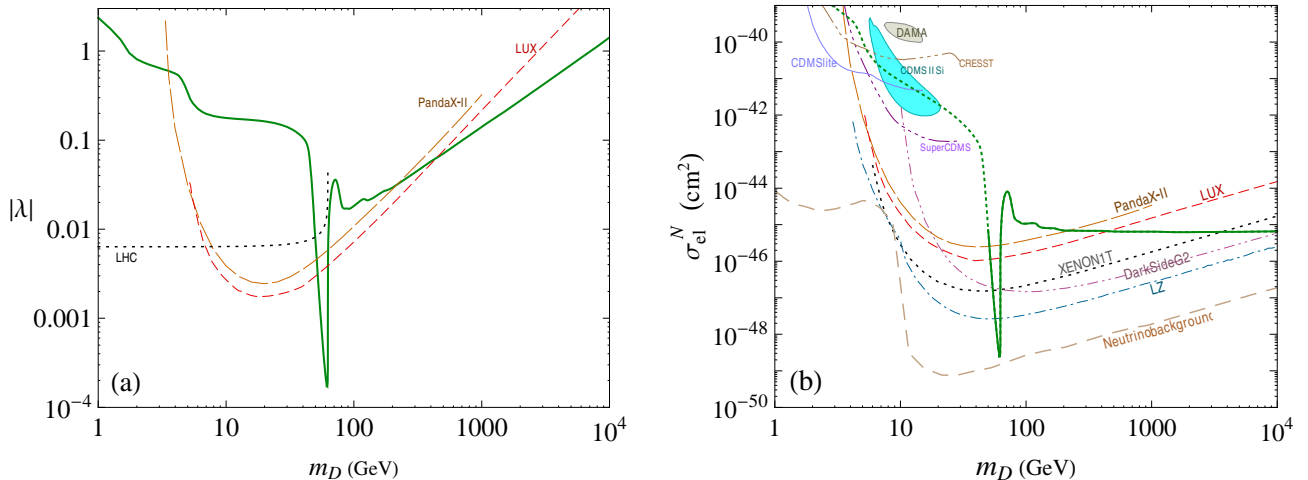


FIG. 2: (a) The magnitude of the darkon-Higgs coupling λ satisfying the relic abundance constraint versus the darkon mass m_D in the SM+D (green curve) compared to the upper limits inferred from LHC data on the Higgs invisible decay (black dotted curve) and from the latest LUX (red dashed curve) and PandaX-II (orange dashed curve) searches. (b) The corresponding darkon-nucleon cross-section σ_{el}^N (green curve) compared to the same current data and future potential limits as in Fig. 1(a). The dotted portion of the green curve is excluded by the LHC bound in (a).

resonance region almost touches the expected limit of DM direct detection due to coherent neutrino scattering backgrounds. We also notice that the planned XENON1T, DarkSide G2, and LZ experiments [12] can probe the dip much further, but not all the way down. Thus, to exclude the dip completely a more sensitive machine will be needed. For darkon masses above 450 GeV, tests will be available from the ongoing PandaX-II as well as the forthcoming quests: particularly, XENON1T, DarkSide G2, and LZ can cover up to ~ 3.5 , 10, and a few tens TeV, respectively.

III. CONSTRAINTS ON THDM II+D

There are different types of the two-Higgs-doublet model (THDM), depending on how the two Higgs doublets, H_1 and H_2 , couple to SM fermions [37, 38]. In the THDM I, only one of the doublets is responsible for endowing mass to all the fermions. In the THDM II, the up-type fermions get mass from only one of the Higgs doublets, say H_2 , and the down-type fermions from the other doublet. In the THDM III, both H_1 and H_2 give masses to all the fermions.

Since only one Higgs doublet generates all of the fermion masses in the THDM I, the couplings of each of the CP -even Higgs bosons to fermions are the same as in the SM, up to an overall scaling factor. Therefore, the couplings of the 125-GeV Higgs, h , in the THDM I slightly enlarged with the addition of a darkon are similar to those in the SM+D treated in the previous section, and consequently for $m_D < m_h/2$ the modifications cannot readily ease the restraints from the DM direct searches and LHC quest for the Higgs invisible decay. Combining a darkon with the THDM III instead could provide the desired ingredients to help overcome these obstacles [28], but

the model possesses too many parameters to be predictable, some of which give rise to undesirable flavor-changing neutral-Higgs transitions at tree level. For these reasons, in the remainder of the section we concentrate on the THDM II plus the darkon (THDMII+D).

In the THDMII+D, the fermion sector is no different from that in the THDMII, with the Yukawa interactions being described by [37, 38]

$$\mathcal{L}_Y = -\overline{Q}_{j,L}(\lambda_2^u)_{jl}\tilde{H}_2\mathcal{U}_{l,R} - \overline{Q}_{j,L}(\lambda_1^d)_{jl}H_1\mathcal{D}_{l,R} - \overline{L}_{j,L}(\lambda_1^\ell)_{jl}H_1E_{l,R} + \text{H.c.}, \quad (7)$$

where summation over $j, l = 1, 2, 3$ is implicit, $Q_{j,L}$ ($L_{j,L}$) represents left-handed quark (lepton) doublets, $\mathcal{U}_{l,R}$ and $\mathcal{D}_{l,R}$ ($E_{l,R}$) denote right-handed quark (charged lepton) fields, $\tilde{H}_{1,2} = i\tau_2 H_{1,2}^*$ with τ_2 being the second Pauli matrix, and $\lambda^{u,d,\ell}$ are 3×3 matrices for the Yukawa couplings. This Lagrangian respects the discrete symmetry, Z_2 , under which $H_2 \rightarrow -H_2$ and $\mathcal{U}_R \rightarrow -\mathcal{U}_R$, while all the other fields are not affected. Thus, Z_2 prohibits the combinations $\overline{Q}_L\tilde{H}_1\mathcal{U}_R$, $\overline{Q}_L H_2\mathcal{D}_R$, $\overline{L}_L H_2 E_R$, and their Hermitian conjugates from occurring in \mathcal{L}_Y .

The longevity of the darkon as the DM in the THDMII+D is maintained by another discrete symmetry, Z'_2 , under which $D \rightarrow -D$, whereas all the other fields are Z'_2 even. Consequently, being a real field and transforming as a singlet under the SM gauge group, D has no renormalizable interactions with SM fermions or gauge bosons, like in the SM+D.

The renormalizable Lagrangian of the model, $\mathcal{L} \supset -\mathcal{V}_D - \mathcal{V}_H$, contains the scalar potential terms [27]

$$\begin{aligned} \mathcal{V}_D &= \frac{m_0^2}{2}D^2 + \frac{\lambda_D}{4}D^4 + (\lambda_{1D}H_1^\dagger H_1 + \lambda_{2D}H_2^\dagger H_2)D^2, \\ \mathcal{V}_H &= m_{11}^2 H_1^\dagger H_1 + m_{22}^2 H_2^\dagger H_2 - (m_{12}^2 H_1^\dagger H_2 + \text{H.c.}) + \frac{\lambda_1}{2}(H_1^\dagger H_1)^2 + \frac{\lambda_2}{2}(H_2^\dagger H_2)^2 \\ &\quad + \lambda_3 H_1^\dagger H_1 H_2^\dagger H_2 + \lambda_4 H_1^\dagger H_2 H_2^\dagger H_1 + \frac{\lambda_5}{2}[(H_1^\dagger H_2)^2 + \text{H.c.}], \end{aligned} \quad (8)$$

where \mathcal{V}_H is the usual THDM II potential [37, 38]. Because of Z_2 , the combinations $H_1^\dagger H_2 D^2$, $H_1^\dagger H_1 H_1^\dagger H_2$, $H_1^\dagger H_2 H_2^\dagger H_2$, and their Hermitian conjugates are forbidden from appearing in Eq. (8). However, in \mathcal{V}_H we have included the m_{12}^2 terms which softly break Z_2 and are important in relaxing the upper bounds on the Higgs masses [38]. In contrast, Z'_2 , which guarantees the darkon stability, is exactly conserved. The Hermiticity of $\mathcal{V}_{D,H}$ implies that the parameters $m_{0,11,22}^2$ and $\lambda_{D,1D,2D,1,2,3,4}$ are real. We assume $\mathcal{V}_{D,H}$ to be CP invariant, and so m_{12}^2 and λ_5 are also real parameters.

The $\lambda_{1D,2D}$ terms in Eq. (8) play a crucial role in the determination of the relic density, which follows from darkon annihilation into the other particles via interactions with the Higgs bosons. To address this in more detail, we first decompose the Higgs doublets as

$$H_r = \frac{1}{\sqrt{2}} \begin{pmatrix} \sqrt{2}h_r^+ \\ v_r + h_r^0 + iI_r^0 \end{pmatrix}, \quad r = 1, 2, \quad (9)$$

where $v_{1,2}$ are the VEVs of $H_{1,2}$, respectively, and connected to the electroweak scale $v \simeq 246$ GeV by $v_1 = v \cos \beta$ and $v_2 = v \sin \beta$. The H_r components h_r^+ , h_r^0 , and I_r^0 are related to the physical

Higgs bosons h , H , A , and H^+ and the would-be Goldstone bosons w^+ and z by

$$\begin{aligned} \begin{pmatrix} h_1^+ \\ h_2^+ \end{pmatrix} &= \begin{pmatrix} c_\beta & -s_\beta \\ s_\beta & c_\beta \end{pmatrix} \begin{pmatrix} w^+ \\ H^+ \end{pmatrix}, & \begin{pmatrix} I_1^0 \\ I_2^0 \end{pmatrix} &= \begin{pmatrix} c_\beta & -s_\beta \\ s_\beta & c_\beta \end{pmatrix} \begin{pmatrix} z \\ A \end{pmatrix}, \\ \begin{pmatrix} h_1^0 \\ h_2^0 \end{pmatrix} &= \begin{pmatrix} c_\alpha & -s_\alpha \\ s_\alpha & c_\alpha \end{pmatrix} \begin{pmatrix} H \\ h \end{pmatrix}, & c_{\mathcal{X}} &= \cos \mathcal{X}, & s_{\mathcal{X}} &= \sin \mathcal{X}, \end{aligned} \quad (10)$$

where \mathcal{X} is any angle or combination of angles. The w^\pm and z will be eaten by the W^\pm and Z bosons, respectively.

After electroweak symmetry breaking, we can then express the relevant terms in $\mathcal{V} = \mathcal{V}_D + \mathcal{V}_H$ involving the physical bosons as

$$\begin{aligned} \mathcal{V} \supset & \frac{1}{2} m_D^2 D^2 + (\lambda_h h + \lambda_H H) D^2 v \\ & + \frac{1}{2} (\lambda_{hh} h^2 + 2\lambda_{hH} hH + \lambda_{HH} H^2 + \lambda_{AA} A^2 + 2\lambda_{H^+H^-} H^+ H^-) D^2 \\ & + \left(\frac{1}{6} \lambda_{hhh} h^3 + \frac{1}{2} \lambda_{hhH} h^2 H + \frac{1}{2} \lambda_{hHH} h H^2 + \frac{1}{2} \lambda_{hAA} h A^2 + \lambda_{H^+H^-} H^+ H^- \right) h v \\ & + \left(\frac{1}{6} \lambda_{HHH} H^3 + \frac{1}{2} \lambda_{HAA} H^2 A + \lambda_{H^+H^-} H^+ H^- \right) H v, \end{aligned} \quad (11)$$

where $m_D^2 = m_0^2 + (\lambda_{1D} c_\beta^2 + \lambda_{2D} s_\beta^2) v^2$,

$$\begin{aligned} \lambda_h &= \lambda_{2D} c_\alpha s_\beta - \lambda_{1D} s_\alpha c_\beta, & \lambda_H &= \lambda_{1D} c_\alpha c_\beta + \lambda_{2D} s_\alpha s_\beta, \\ \lambda_{hh} &= \lambda_{1D} s_\alpha^2 + \lambda_{2D} c_\alpha^2, & \lambda_{HH} &= \lambda_{1D} c_\alpha^2 + \lambda_{2D} s_\alpha^2, \\ \lambda_{hH} &= (\lambda_{2D} - \lambda_{1D}) c_\alpha s_\alpha, & \lambda_{AA} &= \lambda_{H^+H^-} = \lambda_{1D} s_\beta^2 + \lambda_{2D} c_\beta^2, \end{aligned} \quad (12)$$

and the cubic couplings λ_{XYZ} are listed in Appendix A. There is no AD^2 term under the assumed CP invariance. Since m_0 and $\lambda_{1,2}$ are free parameters, so are m_D and $\lambda_{h,H}$. The quartic couplings of the darkon to the Higgs bosons can then be related to $\lambda_{h,H}$ by

$$\begin{aligned} \lambda_{hh} &= \left(\frac{c_\alpha^3}{s_\beta} - \frac{s_\alpha^3}{c_\beta} \right) \lambda_h + \frac{s_{2\alpha} c_{\beta-\alpha}}{s_{2\beta}} \lambda_H, & \lambda_{HH} &= \left(\frac{c_\alpha^3}{c_\beta} + \frac{s_\alpha^3}{s_\beta} \right) \lambda_H - \frac{s_{2\alpha} s_{\beta-\alpha}}{s_{2\beta}} \lambda_h, \\ \lambda_{hH} &= \frac{s_{2\alpha}}{s_{2\beta}} (\lambda_h c_{\beta-\alpha} - \lambda_H s_{\beta-\alpha}), & \lambda_{AA} = \lambda_{H^+H^-} &= \frac{c_\alpha c_\beta^3 - s_\alpha s_\beta^3}{c_\beta s_\beta} \lambda_h + \frac{c_\alpha s_\beta^3 + s_\alpha c_\beta^3}{c_\beta s_\beta} \lambda_H. \end{aligned} \quad (13)$$

Since h and H couple directly to the weak bosons, we need to include the annihilation channels $DD \rightarrow W^+W^-, ZZ$ if kinematically permitted. The pertinent interactions are given by

$$\mathcal{L} \supset (2m_W^2 W^{+\mu} W_\mu^- + m_Z^2 Z^\mu Z_\mu) \left(k_V^h \frac{h}{v} + k_V^H \frac{H}{v} \right), \quad k_V^h = s_{\beta-\alpha}, \quad k_V^H = c_{\beta-\alpha}. \quad (14)$$

The scattering of the darkon off a nucleon $\mathcal{N} = p$ or n is generally mediated at the quark level by h and H and hence depends not only on the darkon-Higgs couplings $\lambda_{h,H}$, but also on the effective Higgs-nucleon coupling $g_{\mathcal{N}\mathcal{N}\mathcal{H}}$ defined by

$$\mathcal{L}_{\mathcal{N}\mathcal{N}\mathcal{H}} = -g_{\mathcal{N}\mathcal{N}\mathcal{H}} \bar{\mathcal{N}} \mathcal{N} \mathcal{H}, \quad \mathcal{H} = h, H. \quad (15)$$

This originates from the quark-Higgs terms in Eq. (7) given by

$$\mathcal{L}_Y \supset -\sum_q k_q^{\mathcal{H}} m_q \bar{q} q \frac{\mathcal{H}}{v}, \quad k_{c,t}^{\mathcal{H}} = k_u^{\mathcal{H}}, \quad k_{s,b}^{\mathcal{H}} = k_d^{\mathcal{H}}, \quad (16)$$

where the sum is over all quarks, $q = u, d, s, c, b, t$, and

$$k_u^h = \frac{c_\alpha}{s_\beta}, \quad k_d^h = -\frac{s_\alpha}{c_\beta}, \quad k_u^H = \frac{s_\alpha}{s_\beta}, \quad k_d^H = \frac{c_\alpha}{c_\beta}. \quad (17)$$

It follows that [39]

$$g_{\mathcal{N}\mathcal{N}\mathcal{H}} = \frac{m_{\mathcal{N}}}{v} \left[(f_u^{\mathcal{N}} + f_c^{\mathcal{N}} + f_t^{\mathcal{N}}) k_u^{\mathcal{H}} + (f_d^{\mathcal{N}} + f_s^{\mathcal{N}} + f_b^{\mathcal{N}}) k_d^{\mathcal{H}} \right], \quad (18)$$

where $f_q^{\mathcal{N}}$ is defined by the matrix element $\langle \mathcal{N} | m_q \bar{q} q | \mathcal{N} \rangle = f_q^{\mathcal{N}} m_{\mathcal{N}} \bar{u}_{\mathcal{N}} u_{\mathcal{N}}$ with $u_{\mathcal{N}}$ being the Dirac spinor for \mathcal{N} and $m_{\mathcal{N}}$ its mass. Employing the values $f_q^{\mathcal{N}}$ for the different quarks listed in Appendix A, we find

$$g_{pp\mathcal{H}} = (0.5631 k_u^{\mathcal{H}} + 0.5599 k_d^{\mathcal{H}}) \times 10^{-3}, \quad g_{nn\mathcal{H}} = (0.5481 k_u^{\mathcal{H}} + 0.5857 k_d^{\mathcal{H}}) \times 10^{-3}. \quad (19)$$

Setting $k_{u,d}^h = 1$ in these formulas, we reproduce the SM values $g_{pp\mathcal{H}}^{\text{SM}} \simeq 0.0011$ quoted in the last section. However, if $k_{u,d}^{\mathcal{H}}$ are not close to unity, $g_{pp\mathcal{H}}$ and $g_{nn\mathcal{H}}$ can be very dissimilar, breaking isospin symmetry substantially. Particularly, they have different zeros, $k_d^{\mathcal{H}} \simeq -1.01 k_u^{\mathcal{H}}$ and $k_d^{\mathcal{H}} \simeq -0.936 k_u^{\mathcal{H}}$, respectively.

This suggests that to evaluate DM collisions with nucleons in the THDMII+D it is more appropriate to work with either the darkon-proton or darkon-neutron cross-section (σ_{el}^p or σ_{el}^n , respectively) rather than the darkon-nucleon one under the assumption of isospin conservation. The calculated $\sigma_{\text{el}}^{p,n}$ can then be compared to their empirical counterparts which are converted from the measured σ_{el}^N using the relations [18, 19]

$$\sigma_{\text{el}}^N \sum_i \eta_i \mu_{A_i}^2 A_i^2 = \sigma_{\text{el}}^p \sum_i \eta_i \mu_{A_i}^2 [\mathcal{Z} + (A_i - \mathcal{Z}) f_n / f_p]^2, \quad \sigma_{\text{el}}^n = \sigma_{\text{el}}^p f_n^2 / f_p^2, \quad (20)$$

where the sums are over the isotopes of the element in the target material with which the DM interacts dominantly, η_i (A_i) represent the fractional abundances (the nucleon numbers) of the isotopes,⁴ $\mu_{A_i} = m_{A_i} m_D / (m_{A_i} + m_D)$, with m_{A_i} being the i th isotope's mass, \mathcal{Z} denotes the proton number of the element, and f_n / f_p is fixed under certain assumptions. For illustration, from Eq. (20) we graph $\sigma_{\text{el}}^N / \sigma_{\text{el}}^p$ as a function f_n / f_p for a few target materials (silicon, argon, and xenon) in Fig. 3, where the curves are not sensitive to the darkon masses in our range of interest. Thus, if there is no isospin violation, $f_n = f_p$ leading to $\sigma_{\text{el}}^p = \sigma_{\text{el}}^N$. On the other hand, for DM with maximal xenophobia, $f_n / f_p = -0.70$, and with this number we arrived at Fig. 1(b) from Fig. 1(a). More generally, σ_{el}^p can be bigger or smaller than σ_{el}^N if $f_n \neq f_p$, but completely destructive interference on the right-hand side of the first relation in Eq. (20) yielding $\sigma_{\text{el}}^N / \sigma_{\text{el}}^p = 0$ is not achievable if the element has more than one naturally abundant isotope.

⁴ A recent list of isotopic abundances can be found in [40].

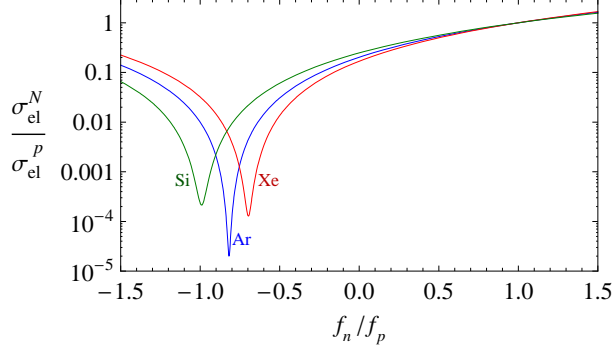


FIG. 3: Dependence of $\sigma_{\text{el}}^N / \sigma_{\text{el}}^p$ on f_n / f_p according to Eq. (20) for silicon, argon, and xenon targets.

If both the h and H couplings to the darkon are nonzero, the cross section of the darkon- \mathcal{N} scattering $DN \rightarrow DN$ is

$$\sigma_{\text{el}}^{\mathcal{N}} = \frac{m_{\mathcal{N}}^2 v^2}{\pi (m_D + m_{\mathcal{N}})^2} \left(\frac{\lambda_h g_{\mathcal{N}\mathcal{N}h}}{m_h^2} + \frac{\lambda_H g_{\mathcal{N}\mathcal{N}H}}{m_H^2} \right)^2 \quad (21)$$

for momentum transfers small relative to $m_{h,H}$ and $\mathcal{N} = p$ or n . Given that $g_{\mathcal{N}\mathcal{N}\mathcal{H}}$ depends on $k_{u,d}^{\mathcal{H}}$ according to Eq. (18), it may be possible to make $g_{\mathcal{N}\mathcal{N}\mathcal{H}}$ sufficiently small with a suitable choice of $k_d^{\mathcal{H}} / k_u^{\mathcal{H}}$ to allow $\sigma_{\text{el}}^{\mathcal{N}}$ to avoid its experimental limit [29], at least for some of the m_D values. Moreover, the $\lambda_{h,H}$ terms in Eq. (21) may (partially) cancel each other to reduce $\sigma_{\text{el}}^{\mathcal{N}}$ as well. These are attractive features of the THDMII+D that the SM+D does not possess.

Since there are numerous different possibilities in which h and H may contribute to darkon interactions with SM particles in the THDM+D, hereafter for definiteness and simplicity we focus on a couple of scenarios in which h is the 125-GeV Higgs boson and the other Higgs bosons are heavier, $m_h < m_{H,A,H^\pm}$. In addition, we assume specifically that either H or h has a vanishing coupling to the darkon, $\lambda_H = 0$ or $\lambda_h = 0$, respectively. As a consequence, either h or H alone serves as the portal between the DM and SM particles, and so we now have $f_n / f_p = g_{nn\mathcal{H}} / g_{pp\mathcal{H}}$, upon neglecting the n - p mass difference.

If we take $g_{nn\mathcal{H}} / g_{pp\mathcal{H}} = -0.70$, which corresponds to the xenophobic limit, using Eq. (19) we get $r_k^{\mathcal{H}} \equiv k_d^{\mathcal{H}} / k_u^{\mathcal{H}} = -0.96$, where $r_k^h = -\tan \alpha \tan \beta$ and $r_k^H = \cot \alpha \tan \beta$ from Eq. (17). Nevertheless, as we see later on, despite the strongest constraints to date from xenon-based detectors, higher $r_k^{\mathcal{H}}$ values are still compatible with the data and hence the darkon can still avoid extreme xenophobia. The choices for α and β , however, need to comply with further restraints on $k_{d,u,V}^h$, as specified below.

Given that LHC measurements have been probing the Higgs couplings to SM fermions and electroweak bosons, we need to take into account the resulting restrictions on potential new physics in the couplings. A modification to the $h \rightarrow X\bar{X}$ interaction with respect to its SM expectation can be parameterized by κ_X defined by $\kappa_X^2 = \Gamma_{h \rightarrow X\bar{X}} / \Gamma_{h \rightarrow X\bar{X}}^{\text{SM}}$. Assuming that $|\kappa_{W,Z}| \leq 1$ and the Higgs total width can get contributions from decay modes beyond the SM, the ATLAS and CMS Collaborations have performed simultaneous fits to their Higgs data to

extract [34]

$$\begin{aligned} \kappa_W &= 0.90 \pm 0.09, & \kappa_t &= 1.43_{-0.22}^{+0.23}, & |\kappa_b| &= 0.57 \pm 0.16, & |\kappa_\gamma| &= 0.90_{-0.09}^{+0.10}, \\ \kappa_Z &= 1.00_{-0.08}, & |\kappa_g| &= 0.81_{-0.10}^{+0.13}, & |\kappa_\tau| &= 0.87_{-0.11}^{+0.12}, \end{aligned} \quad (22)$$

where [34] $\kappa_\gamma^2 = 0.07 \kappa_t^2 + 1.59 \kappa_W^2 - 0.66 \kappa_t \kappa_W$. In the THDM II context, we expect these numbers to respect within one sigma the relations $k_V^h = \kappa_W = \kappa_Z$, $k_u^h = \kappa_t \simeq \kappa_g$, and $k_d^h = \kappa_b = \kappa_\tau$, although the $\kappa_{t,g}$ ($\kappa_{b,\tau}$) numbers above overlap only at the two-sigma level. Accordingly, pending improvement in the precision of these parameters from future data, based on Eq. (22) we may impose

$$0.81 \leq k_V^h \leq 1, \quad 0.71 \leq k_u^h \leq 1.66, \quad 0.41 \leq |k_d^h| \leq 0.99, \quad 0.81 \leq |k_\gamma^h| \leq 1, \quad (23)$$

where k_γ^h incorporates the loop contribution of H^\pm to $h \rightarrow \gamma\gamma$, and so $k_\gamma^h \rightarrow \kappa_\gamma$ if the impact of H^\pm is vanishing. Explicitly

$$k_\gamma^h = 0.264 k_u^h - 1.259 k_V^h + 0.151 \frac{\lambda_{hH^+H^-} v^2}{2m_{H^\pm}^2} A_0^{\gamma\gamma} (4m_{H^\pm}^2/m_h^2), \quad (24)$$

where $A_0^{\gamma\gamma}$ is a loop function whose expression can be found in the literature (*e.g.*, [41]). The effect of the $\lambda_{hH^+H^-}$ term in k_γ^h turns out to be somewhat minor in our examples. To visualize the impact of the limitations in Eq. (23), we plot in Fig. 4 the (red) regions representing the α and β parameter space satisfying them.

Before proceeding to our specific scenarios of choice, we remark that in the alignment limit, $\beta = \alpha + \pi/2$, we recover the SM+D darkon parameters,

$$m_D^2 = m_0^2 + \lambda_h v^2, \quad \lambda_{hh} = \lambda_h \quad (25)$$

with $\lambda_h = \lambda$. Furthermore, in this limit the h couplings become SM-like,

$$\lambda_{hhh} = \frac{3m_h^2}{v^2}, \quad k_V^h = 1, \quad k_q^h = 1. \quad (26)$$

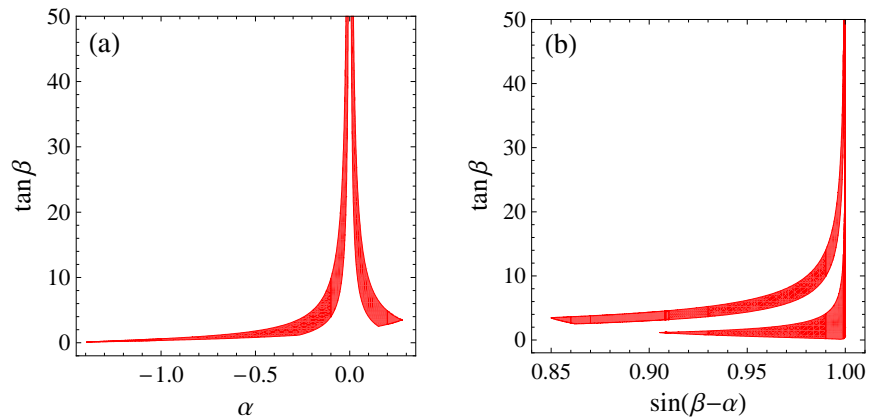


FIG. 4: Regions of $\tan \beta$ versus (a) α and (b) $\sin(\beta - \alpha)$ which obey the restrictions in Eq. (23).

A. $\lambda_H = 0$

In this case, the cross section of the darkon annihilation into THDM particles is

$$\sigma_{\text{ann}} = \sigma(DD \rightarrow h^* \rightarrow X_{\text{SM}}) + \sum_{\mathbf{s}_1 \mathbf{s}_2} \sigma(DD \rightarrow \mathbf{s}_1 \mathbf{s}_2), \quad (27)$$

where the first term on the right-hand side is equal to its SM+D counterpart in Eq. (3), except λ is replaced by λ_h and the h couplings to fermions and gauge bosons are multiplied by the relevant $k_{u,d,V}^h$ factors mentioned earlier, and the sum is over $\mathbf{s}_1 \mathbf{s}_2 = hh, hH, HH, AA, H^+ H^-$ with only kinematically allowed channels contributing. The formulas for $\sigma(DD \rightarrow \mathbf{s}_1 \mathbf{s}_2)$ have been relegated to Appendix A. Hence, though not the portal between the DM and SM particles in this scenario, H can still contribute to the darkon relic abundance via $DD \rightarrow \mathbf{s}_1 \mathbf{s}_2$, along with A and H^\pm .

Once λ_h has been extracted from the relic density data and $g_{\mathcal{N}\mathcal{N}h}$ calculated with the α and β choices consistent with Eq. (17), we can predict the darkon- \mathcal{N} cross-section. From now on, we work exclusively with the darkon-proton one,

$$\sigma_{\text{el}}^p = \frac{\lambda_h^2 g_{pph}^2 m_p^2 v^2}{\pi (m_D + m_p)^2 m_h^4}. \quad (28)$$

This is to be compared to its empirical counterparts derived from the σ_{el}^N data using Eq. (20) with $f_n/f_p = g_{nmh}/g_{pph}$. There are other restrictions that we need to take into account.

As in the SM+D, for $m_D < m_h/2$ the invisible channel $h \rightarrow DD$ is open and has a rate given by Eq. (4), with λ being replaced by λ_h . The branching fraction of $h \rightarrow DD$ must then be consistent with the LHC measurement on the Higgs invisible decay, and so for this darkon mass range we again impose the bound in Eq. (5).

Since the extra Higgs particles in the THDM exist due to the second doublet being present, they generally affect the so-called oblique electroweak parameters S and T which encode the impact of new physics coupled the standard $SU(2)_L$ gauge boson [42]. Thus the new scalars must also comply with the experimental constraints on these quantities. To ensure this, we employ the pertinent formulas from Ref. [43] and the S and T data from Ref. [1].

Lastly, the parameters of the scalar potential $\mathcal{V} = \mathcal{V}_D + \mathcal{V}_H$ in Eq. (8) need to fulfill a number of theoretical conditions. The quartic couplings in \mathcal{V} cannot be too big individually, for otherwise the theory will no longer be perturbative. Another requirement is that \mathcal{V} must be stable, implying that it has to be bounded from below to prevent it from becoming infinitely negative for arbitrarily large fields. It is also essential to ensure that the (tree level) amplitudes for scalar-scalar scattering at high energies do not violate unitarity constraints. We address these conditions in more detail in Appendix B. They can be consequential in restraining parts of the model parameter space, especially for m_D less than $\mathcal{O}(100 \text{ GeV})$, as some of our examples will later demonstrate.

To illustrate the viable parameter space in this scenario, in the second to seventh columns of Table I we put together a few sample sets of input parameters which are consistent with Eq. (23) and the requirements described in the last two paragraphs. The eighth to twelfth columns contain the resulting values of several quantities. With the input numbers from Set 1 in the table, we

Set	α	β	$\frac{m_H}{\text{GeV}}$	$\frac{m_A}{\text{GeV}}$	$\frac{m_{H^\pm}}{\text{GeV}}$	$\frac{m_{12}^2}{\text{GeV}^2}$	k_V^h	k_u^h	$\frac{k_d^h}{k_u^h}$	k_V^H	k_u^H	k_d^H	$\frac{g_{pph}}{10^{-5}}$	$\frac{f_n}{f_p}$
1	0.117	1.428	470	500	550	31000	0.966	1.003	-0.818	0.257	0.118	6.98	10.6	+0.658
2	0.141	1.422	550	520	540	44000	0.958	1.001	-0.947	0.286	0.142	6.68	3.29	-0.197
3	0.206	1.357	515	560	570	55000	0.913	1.002	-0.962	0.408	0.209	4.61	2.42	-0.646

TABLE I: Sample values of input parameters α , β , m_{H,A,H^\pm} , and m_{12}^2 in the $\lambda_H = 0$ scenario and the resulting values of several quantities, including $f_n/f_p = g_{nnh}/g_{pph}$.

show in Fig. 5(a) the λ_h region evaluated from the observed relic density. We also display the upper limits on λ_h inferred from Eq. (5) for the $h \rightarrow DD$ limit (black dotted curve), from the latest LUX [2] and PandaX-II [3] searches, and from the aforementioned theoretical demands for perturbativity, potential stability, and unitarity.

The plot in Fig. 5(b) exhibits the corresponding prediction for σ_{el}^p (green curve) compared to its empirical counterparts obtained from the data depicted in Fig. 1(a) by employing Eq. (20) with $f_n/f_p = 0.658$ from Set 1 in Table I. One observes that the $m_D < 50$ GeV region, represented by the dotted section of the green curve, is incompatible with the LHC constraint on $h \rightarrow DD$ and a portion of it is also excluded by LUX and PandaX-II. The green solid curve is below all of the existing limits from direct searches and for a narrow range of m_D lies not far under the LUX line. Upcoming quests with XENON1T as well as DarkSide G2 will apparently be sensitive to only a small section of the green solid curve, below 100 GeV, whereas LZ can be expected to reach more of it, from about 63 to 170 GeV.

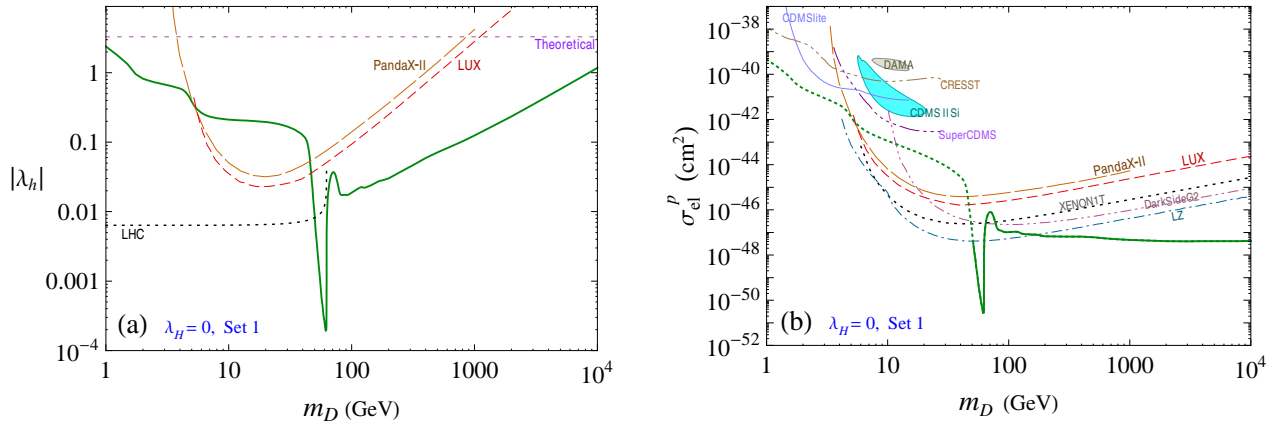


FIG. 5: (a) The darkon- h coupling λ_h consistent with the relic data (green curve) versus darkon mass in the THDMII+D with $\lambda_H = 0$ and input numbers from Set 1 in Table I. Also plotted are upper limits from the theoretical conditions mentioned in the text (horizontal purple dotted-line), the LHC Higgs invisible decay data (black dotted-curve), and the latest LUX (red dashed-curve) and PandaX-II (orange dashed-curve) results. (b) The corresponding darkon-proton cross-section σ_{el}^p (green curve), compared to its counterparts translated from the σ_{el}^N data and projections in Fig. 1(a) using Eq. (20) with f_n/f_p from Set 1 in Table I. The dotted portion of the green curve is excluded by the LHC bound in (a).

For further illustrations, in Fig. 6 we graph analogous results with the input numbers from Sets 2 and 3 in Table I. Their f_n/f_p values are lower than that in Set 1, making the darkon more xenophobic and therefore harder to discover with xenon-based detectors, as can also be deduced from Fig. 3. Especially, in these instances the predictions for σ_{el}^p (green solid curves) are far less than the available experimental bounds and may be out of reach for direct searches in the not-too-distant future.

For a more straightforward comparison between the model predictions and direct search results, which are typically reported in terms of the DM-nucleon cross-section σ_{el}^N , we have converted the calculated σ_{el}^p in Figs. 5 and 6 to the three (green) σ_{el}^N curves in Fig. 7(a) using Eq. (20) with the f_n/f_p values from Table I and assuming that the target material in the detector is xenon. Recalling that the DarkSide G2 experiment will employ an argon target [14], we plot the corresponding predictions for σ_{el}^N assuming an argon target instead in Fig. 7(b), which reveals some visible differences from Fig. 7(a) in the predictions with $f_n/f_p < 0$, as Fig. 3 would imply as well. Also shown are the same data and projections as in Fig. 1(a). From Fig. 7, we can conclude that near-future direct detection experiments will be sensitive to only a rather limited part of the h -portal THDMII+D parameter space. We notice specifically that the predicted σ_{el}^N in much of the $m_D > 100$ GeV region is under the neutrino-background floor.

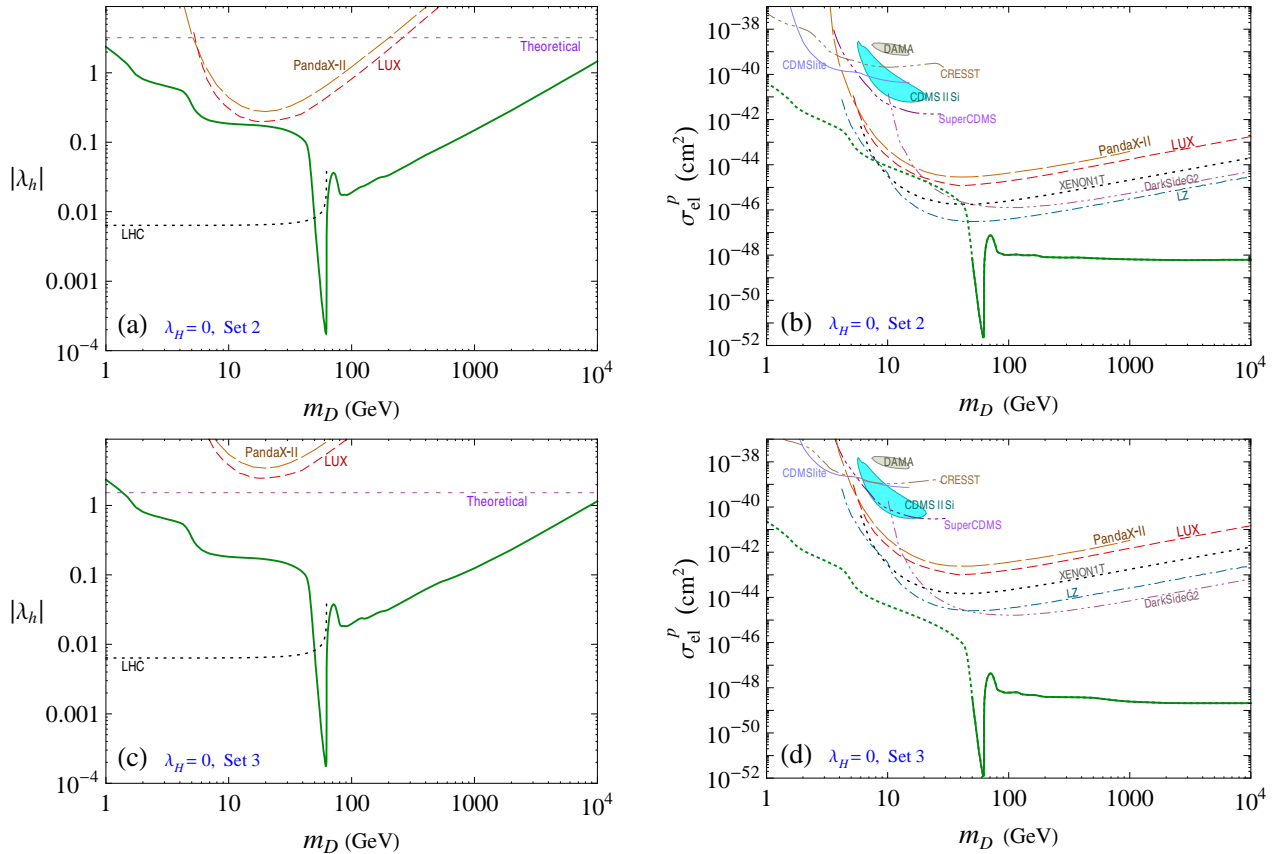


FIG. 6: The same as Fig. 5, except the input parameters are from Set 2 (a,b) and Set 3 (c,d) in Table I.

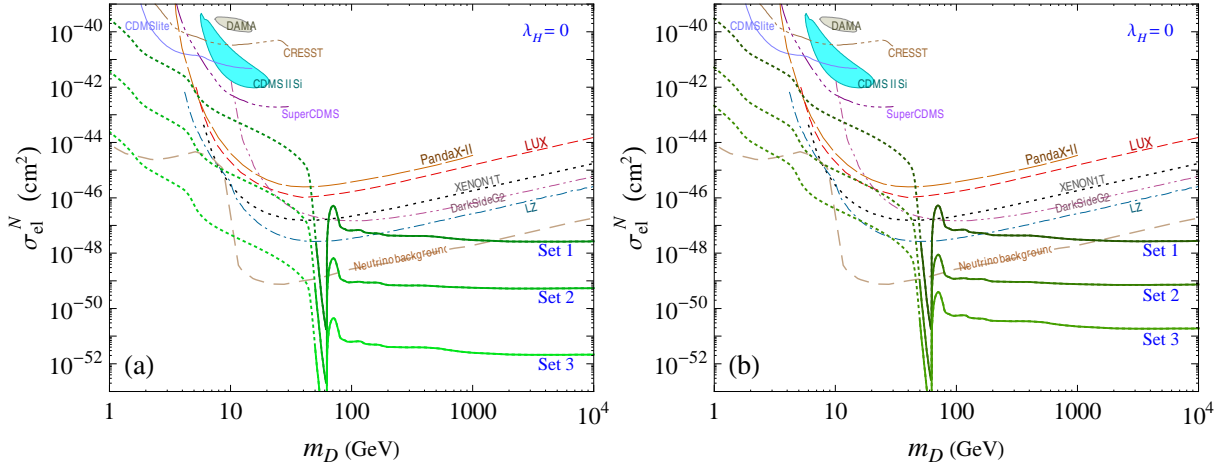


FIG. 7: The predictions for darkon-nucleon cross-section σ_{el}^N (green curves) corresponding to Sets 1-3 in Table I for (a) xenon and (b) argon targets as described in the text, compared to the same data and projections as in Fig. 1(a). The dotted portions of the green curves are excluded as in Figs. 5 and 6.

B. $\lambda_h = 0$

In this scenario, the cross section of the darkon annihilation into THDM particles is

$$\sigma_{\text{ann}} = \sigma(DD \rightarrow H^* \rightarrow X_{\text{SM}}) + \sum_{\mathbf{s}_1 \mathbf{s}_2} \sigma(DD \rightarrow \mathbf{s}_1 \mathbf{s}_2), \quad (29)$$

where

$$\sigma(DD \rightarrow H^* \rightarrow X_{\text{SM}}) = \frac{4\lambda_H^2 v^2}{(m_H^2 - s)^2 + \Gamma_H^2 m_H^2} \frac{\sum_i \Gamma(\tilde{H} \rightarrow X_{i,\text{SM}})}{\sqrt{s - 4m_D^2}}, \quad (30)$$

with \tilde{H} being a virtual H having the same couplings as the physical H and an invariant mass equal to \sqrt{s} , and the sum in σ_{ann} is again over $\mathbf{s}_1 \mathbf{s}_2 = hh, hH, HH, AA, H^+ H^-$. For the H -mediated darkon-proton scattering, $Dp \rightarrow Dp$, the cross section is

$$\sigma_{\text{el}}^p = \frac{\lambda_H^2 g_{ppH}^2 m_p^2 v^2}{\pi (m_D + m_p)^2 m_H^4}. \quad (31)$$

In applying Eq. (20), we set $f_n/f_p = g_{nnH}/g_{ppH}$.

Similarly to the $\lambda_H = 0$ case, here we present three examples, with their respective sets of input numbers being collected in Table II. We also impose the requirements described earlier in this section, except that the LHC information on the decay mode $h \rightarrow \text{invisible}$ is not useful for bounding λ_H . Nevertheless, the theoretical conditions for perturbativity, stability of the potential, and unitarity of high-energy scalar scattering amplitudes turn out to be consequential in disallowing darkon masses less than 100 GeV.

The input numbers from Set 1 (Sets 2 and 3) in Table II lead to the graphs in Fig. 8 (9). In these figures, we see that the $|\lambda_H|$ values extracted from the relic density data tend to be bigger than their λ_h counterparts in the $\lambda_H = 0$ instances. This is because the H -mediated

Set	α	β	$\frac{m_H}{\text{GeV}}$	$\frac{m_A}{\text{GeV}}$	$\frac{m_{H^\pm}}{\text{GeV}}$	$\frac{m_{12}^2}{\text{GeV}^2}$	k_V^h	k_u^h	k_d^h	$k_V^{H^*}$	$k_u^{H^*}$	$\frac{k_d^{H^*}}{k_u^{H^*}}$	$\frac{g_{ppH}}{10^{-5}}$	$\frac{f_n}{f_p}$
1	-0.785	0.738	550	600	650	70000	0.999	1.051	0.955	0.048	-1.051	-0.910	-5.62	+0.281
2	-0.749	0.723	610	750	760	91000	0.995	1.107	0.908	0.099	-1.029	-0.949	-3.26	-0.245
3	-0.676	0.658	590	610	640	60000	0.972	1.276	0.791	0.235	-1.023	-0.964	-2.40	-0.693

TABLE II: Samples values of input parameters α , β , m_{H,A,H^\pm} , and m_{12}^2 in the $\lambda_h = 0$ scenario and the resulting values of several quantities, including $f_n/f_p = g_{nnH}/g_{ppH}$.

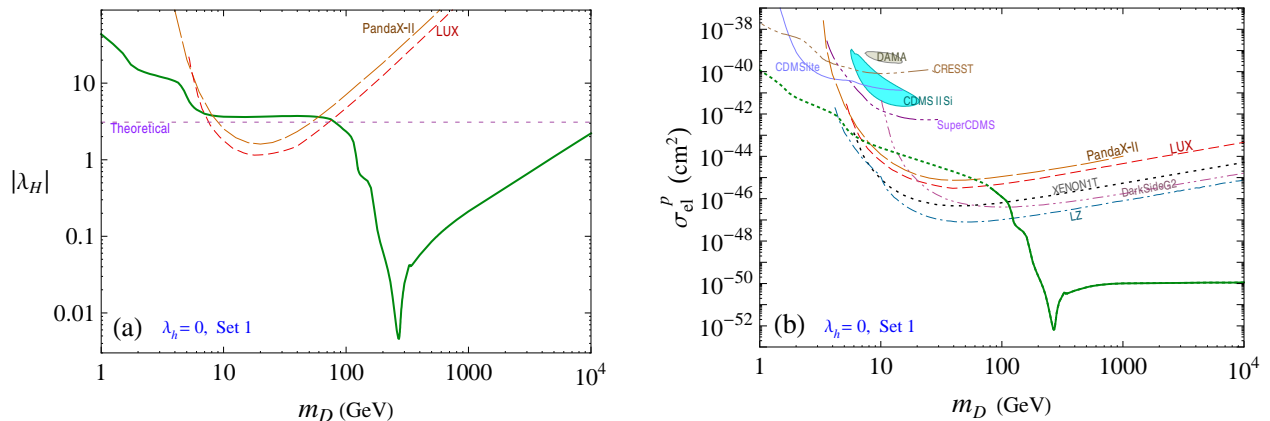


FIG. 8: (a) The darkon- H coupling λ_H versus darkon mass in the THDM II+D with $\lambda_h = 0$ and input numbers from Set 1 in Table II. (b) The corresponding darkon-proton cross-section σ_{el}^p (green curve), compared to its counterparts translated from Fig. 1(a) using Eq. (20) with f_n/f_p from Set 1 in Table II. The dotted portion of the green curve is excluded by the theoretical bound in (a).

annihilation rate is relatively more suppressed due to $m_H > m_h$. As a consequence, more of the low- m_D regions are in conflict with the restrictions from the aforementioned theoretical requirements. Furthermore, in Fig. 8(b), like in Fig. 5(b), there is a small range of the solid green curve, around its leftmost end, that is close to the LUX and PandaX-II limits.

As in the previous subsection, assuming xenon to be the target material, we have translated the predicted σ_{el}^p in Figs. 8 and 9 into the three (green) σ_{el}^N curves in Fig. 10(a) in order to provide a more direct comparison with experimental results. If the target is argon instead and $f_n/f_p < 0$, the σ_{el}^N predictions can be visibly greater, as depicted in Fig. 10(b).

For darkon masses above 100 GeV, the majority of the σ_{el}^N predictions in Fig. 10 appear to lie under the neutrino-background floor, more in these instances than those in the $\lambda_H = 0$ case. Thus, the $\lambda_h = 0$ scenario is likely to be comparatively more challenging to probe with direct searches.

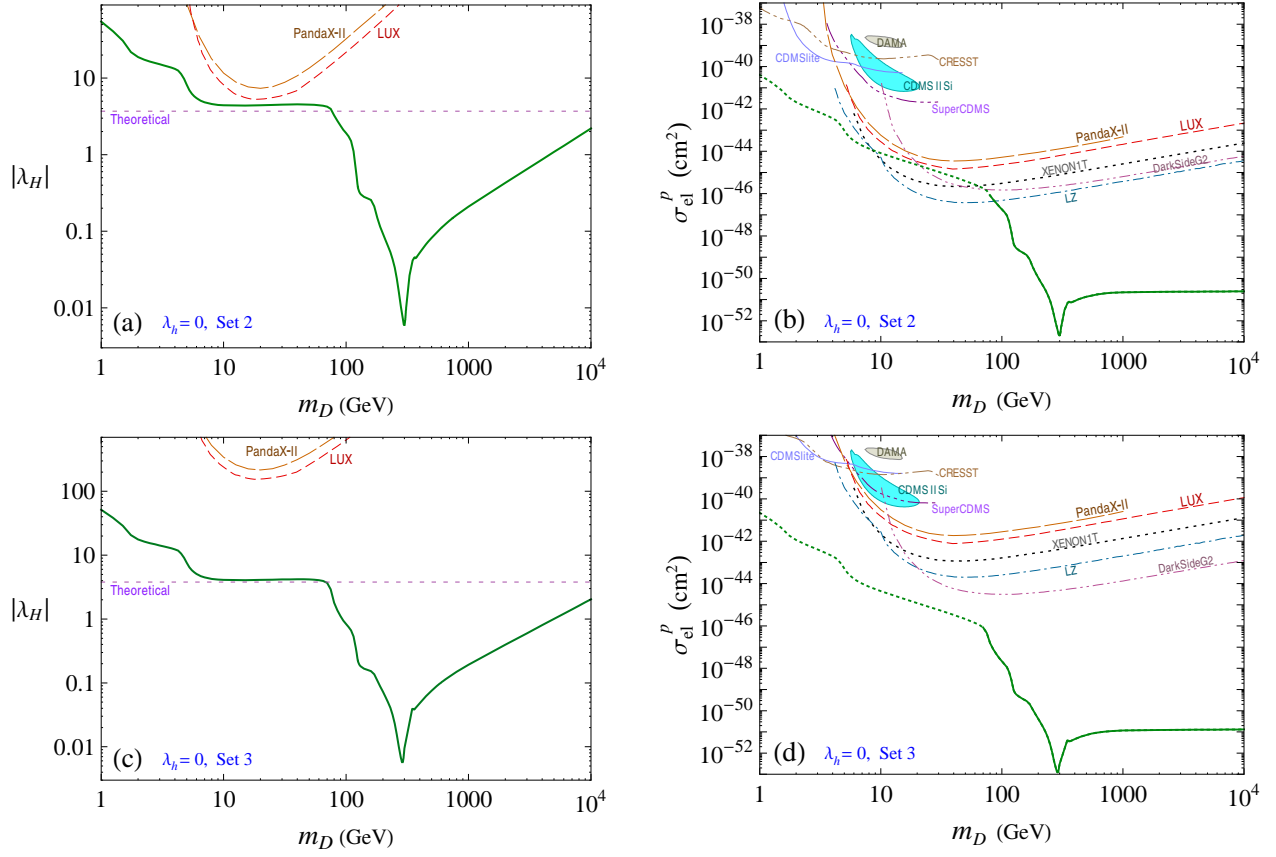


FIG. 9: The same as Fig. 8, except the input parameters are from Set 2 (a,b) and Set 3 (c,d) in Table II.

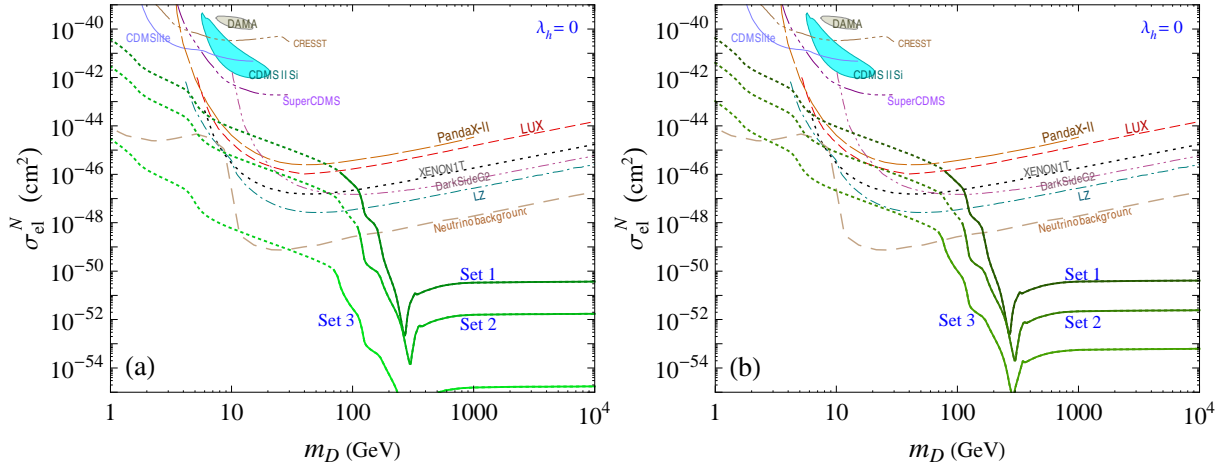


FIG. 10: The predictions for darkon-nucleon cross-section σ_{el}^N (green curves) corresponding to Sets 1-3 in Table II for (a) xenon and (b) argon targets as described in the text, compared to the same data and projections as in Fig. 1(a). The dotted portions of the green curves are excluded as in Figs. 8 and 9.

IV. CONCLUSIONS

We have explored some of the implications of the most recent null results of WIMP DM direct searches by LUX and PandaX-II. For Higgs-portal scalar WIMP DM models, the new limits have eliminated any possibility to accommodate low-mass DM undergoing spin-independent elastic scattering off nucleons that was suggested by the potentially positive results of the DAMA and CDMS II Si experiments, even after invoking the mechanism of isospin violation in DM-nucleon interactions. We have studied particularly how the LUX and PandaX-II results probe the parameter space of the simplest Higgs-portal scalar DM models, namely the SM+D, which is the SM plus a real scalar singlet called darkon, and the THDMII+D, which is the two-Higgs-doublet model of type II combined with a darkon. In the THDMII+D we entertain the possibility that the 125-GeV Higgs boson, h , is the lightest one of the physical members of the scalar doublets. Our analysis takes into account various constraints from LHC data on the Yukawa couplings of h , its couplings to gauge bosons, and its invisible decay mode. Also pertinent are restrictions from oblique electroweak precision measurements and from theoretical considerations regarding perturbativity, vacuum stability, and unitarity. In the SM+D case, h is the only portal between the DM and SM sectors, while in the THDMII+D one or both of the CP -even Higgs bosons, h and the heavier H , can be the portals.

We find that in scenarios with h being the only portal the LHC information on $h \rightarrow$ invisible places a significant restraint on the darkon- h coupling and rules out the $m_D \leq m_h/2$ region, except a small range near the resonance point $m_D = m_h/2$. We also find that for $m_D > m_h/2$ in the SM+D the new LUX and PandaX-II limits exclude masses up to 450 GeV or so, but in the h -portal THDMII+D they can be recovered due to suppression of the Higgs-nucleon coupling, g_{NNh} , at some values of the product $\tan\alpha \tan\beta$. In contrast, in the THDMII+D scenario with H being the sole portal, the $h \rightarrow$ invisible bound does not apply to the much heavier H , and the LUX and PandaX-II limits can be evaded due to suppression of g_{NNH} at some values of $\cot\alpha \tan\beta$. However, in this case our examples demonstrate that the foregoing theoretical requirements are consequential and disallow most of the $m_D < 100$ GeV region. Thus, darkon masses below $m_D \simeq 50$ GeV are ruled out in the SM+D by LHC data and very likely so in the THDMII+D by the LHC and theoretical restrictions. For higher masses, lower parts of the dip around $m_D = m_h/2$ in the h -portal cases will remain viable for the foreseeable future, and beyond the h -resonance area the region up to roughly 3.5, 10, and 20 TeV in the SM+D will be testable by XENON1T, DarkSide G2, and LZ, respectively. For $m_D > 100$ GeV in the THDMII+D there is generally ample parameter space that yields a darkon-nucleon cross-section below the neutrino-background floor and is therefore likely to elude direct detection experiments in the future which lack directional sensitivity. Finally, we point out that the considerable suppression of $g_{NN\mathcal{H}}$ is accompanied by $g_{pp\mathcal{H}}$ and $g_{nn\mathcal{H}}$ manifesting sizable isospin breaking, as illustrated in our examples.

Acknowledgments

This research was supported in part by MOE Academic Excellence Program (Grant No. 102R891505) and NCTS of ROC. X.-G. He was also supported in part by MOST of ROC

(Grant No. MOST104-2112-M-002-015-MY3) and in part by NSFC (Grant Nos. 11175115 and 11575111), Key Laboratory for Particle Physics, Astrophysics and Cosmology, Ministry of Education, and Shanghai Key Laboratory for Particle Physics and Cosmology (SKLPPC) (Grant No. 11DZ2260700) of PRC.

Appendix A: Extra formulas for darkon reactions

To extract the darkon-Higgs coupling which enters the annihilation cross-section σ_{ann} , we employ its thermal average [44]

$$\langle \sigma v_{\text{rel}} \rangle = \frac{x}{8m_D^5 K_2^2(x)} \int_{4m_D^2}^{\infty} ds \sqrt{s} (s - 4m_D^2) K_1(\sqrt{s} x/m_D) \sigma_{\text{ann}}, \quad (\text{A1})$$

where v_{rel} is the relative speed of the DM pair, K_r is the modified Bessel function of the second kind of order r and x can be set to its freeze out value $x = x_f$, which is related to $\langle \sigma v_{\text{rel}} \rangle$ by [45]

$$x_f = \ln \frac{0.038 m_D m_{\text{Pl}} \langle \sigma v_{\text{rel}} \rangle}{\sqrt{g_* x_f}}, \quad (\text{A2})$$

with $m_{\text{Pl}} = 1.22 \times 10^{19}$ GeV being the Planck mass and g_* is the total number of effectively relativistic degrees of freedom below the freeze-out temperature $T_f = m_D/x_f$. In addition, we adopt the numerical values of $\langle \sigma v_{\text{rel}} \rangle$ versus m_D determined in Ref. [46], as well as the latest relic density data $\Omega \hat{h}^2 = 0.1197 \pm 0.0022$ [47], with \hat{h} being the Hubble parameter.

In the THDM II+D, if kinematically allowed, a darkon pair can annihilate into a pair of Higgs bosons, $DD \rightarrow hh, hH, HH, AA, H^+H^-$, induced by the diagrams drawn in Fig. 11. They lead to the cross sections

$$\begin{aligned} \sigma(DD \rightarrow \mathcal{H}\mathcal{H}) &= \frac{\lambda_{\mathcal{H}}^2 v^2}{\beta_D^2 \pi s^2} \left(\frac{\mathcal{M}_{\mathcal{H}\mathcal{H}}}{2} + \frac{2\lambda_{\mathcal{H}}^2 v^2}{2m_{\mathcal{H}}^2 - s} \right) \ln \left| \frac{s - 2m_{\mathcal{H}}^2 - \beta_D \beta_{\mathcal{H}} s}{s - 2m_{\mathcal{H}}^2 + \beta_D \beta_{\mathcal{H}} s} \right| \\ &+ \frac{\beta_{\mathcal{H}}}{\beta_D} \left[\frac{\mathcal{M}_{\mathcal{H}\mathcal{H}}^2}{32\pi s} + \frac{\lambda_{\mathcal{H}}^4 v^4}{\pi(m_{\mathcal{H}}^4 + \beta_{\mathcal{H}}^2 m_D^2 s)} s \right], \end{aligned} \quad (\text{A3})$$

$$\begin{aligned} \sigma(DD \rightarrow hH) &= \frac{\lambda_h \lambda_H v^2}{\beta_D^2 \pi s^2} \left(\mathcal{M}_{hH} + \frac{4\lambda_h \lambda_H v^2}{m_h^2 + m_H^2 - s} \right) \ln \left| \frac{s - m_h^2 - m_H^2 - \beta_D \mathcal{K}^{\frac{1}{2}}(s, m_h^2, m_H^2)}{s - m_h^2 - m_H^2 + \beta_D \mathcal{K}^{\frac{1}{2}}(s, m_h^2, m_H^2)} \right| \\ &+ \frac{\mathcal{K}^{\frac{1}{2}}(s, m_h^2, m_H^2)}{\beta_D \pi s} \left(\frac{\mathcal{M}_{hH}^2}{16s} + \frac{2\lambda_h^2 \lambda_H^2 v^4}{m_h^2 m_H^2 s + \mathcal{K}(s, m_h^2, m_H^2) m_D^2} \right), \end{aligned} \quad (\text{A4})$$

$$\sigma(DD \rightarrow AA) = \frac{\beta_A \mathcal{M}_{AA}^2}{32\beta_D \pi s}, \quad \sigma(DD \rightarrow H^+H^-) = \frac{\beta_{H^\pm} \mathcal{M}_{H^+H^-}^2}{16\beta_D \pi s}, \quad (\text{A5})$$

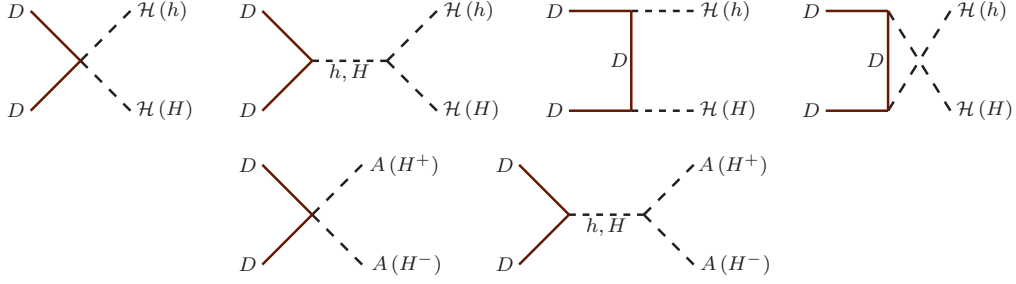


FIG. 11: Feynman diagrams contributing to $DD \rightarrow hh, HH, hH, AA, H^+H^-$.

where \sqrt{s} is the c.m. energy of the darkon pair, $\mathcal{H}\mathcal{H} = hh, HH$,

$$\beta_{\mathbf{x}} = \sqrt{1 - \frac{4m_{\mathbf{x}}^2}{s}}, \quad \mathcal{K}(x, y, z) = x^2 + y^2 + z^2 - 2(xy + yz + xz), \quad (\text{A6})$$

$$\mathcal{M}_{\text{XY}} = 2\lambda_{\text{XY}} + \frac{2\lambda_h \lambda_{h\text{XY}} (s - m_h^2) v^2}{(s - m_h^2)^2 + \Gamma_h^2 m_h^2} + \frac{2\lambda_H \lambda_{H\text{XY}} (s - m_H^2) v^2}{(s - m_H^2)^2 + \Gamma_H^2 m_H^2},$$

$$\text{XY} = hh, hH, HH, AA, H^+H^-, \quad (\text{A7})$$

with λ_{XY} being given by Eq. (12) and

$$\lambda_{hhh} = \frac{c_\alpha^3 c_\beta - s_\alpha^3 s_\beta}{c_\beta s_\beta} \frac{3m_h^2}{v^2} - \frac{3c_{\alpha+\beta} c_{\alpha-\beta}^2 m_{12}^2}{c_\beta^2 s_\beta^2 v^2},$$

$$\lambda_{hhH} = \frac{c_{\beta-\alpha}}{c_\beta s_\beta} \left[s_{2\alpha} \frac{2m_h^2 + m_H^2}{2v^2} + \left(1 - \frac{3s_{2\alpha}}{s_{2\beta}} \right) \frac{m_{12}^2}{v^2} \right] = \lambda_{Hhh},$$

$$\lambda_{hHH} = \frac{s_{\alpha-\beta}}{c_\beta s_\beta} \left[s_{2\alpha} \frac{m_h^2 + 2m_H^2}{2v^2} - \left(1 + \frac{3s_{2\alpha}}{s_{2\beta}} \right) \frac{m_{12}^2}{v^2} \right] = \lambda_{HhH},$$

$$\lambda_{hH^+H^-} = \frac{c_\alpha c_\beta^3 - s_\alpha s_\beta^3}{c_\beta s_\beta} \frac{m_h^2}{v^2} + 2s_{\beta-\alpha} \frac{m_{H^\pm}^2}{v^2} - \frac{c_{\alpha+\beta} m_{12}^2}{c_\beta^2 s_\beta^2 v^2} = \lambda_{hAA} + 2s_{\beta-\alpha} \frac{m_{H^\pm}^2 - m_A^2}{v^2},$$

$$\lambda_{HHH} = \frac{c_\alpha^3 s_\beta + s_\alpha^3 c_\beta}{c_\beta s_\beta} \frac{3m_H^2}{v^2} - \frac{3s_{\alpha+\beta} s_{\alpha-\beta}^2 m_{12}^2}{c_\beta^2 s_\beta^2 v^2},$$

$$\lambda_{HH^+H^-} = \frac{c_\alpha s_\beta^3 + s_\alpha c_\beta^3}{c_\beta s_\beta} \frac{m_H^2}{v^2} + 2c_{\beta-\alpha} \frac{m_{H^\pm}^2}{v^2} - \frac{s_{\alpha+\beta} m_{12}^2}{c_\beta^2 s_\beta^2 v^2} = \lambda_{HAA} + 2c_{\beta-\alpha} \frac{m_{H^\pm}^2 - m_A^2}{v^2}. \quad (\text{A8})$$

In Eqs. (A3) and (A4), we have dropped terms with two powers of $\Gamma_{h,H}$ in the numerators. In the scenarios we look at, Γ_H receives contributions not only from rates of the fermion and gauge-boson decay modes of H , similarly to those of h , but also from

$$\Gamma(H \rightarrow DD) = \frac{\lambda_H^2 v^2}{8\pi m_H} \sqrt{1 - \frac{4m_D^2}{m_H^2}}, \quad \Gamma(H \rightarrow hh) = \frac{\lambda_{hhH}^2 v^2}{8\pi m_H} \sqrt{1 - \frac{4m_h^2}{m_H^2}} \quad (\text{A9})$$

once these channels are open. The $\sigma(DD \rightarrow hh)$ formula in Eq. (A4) is applicable to the SM+D, in which case there is only one coupling for the darkon-Higgs interaction, $\lambda_h = \lambda_{hh} = \lambda$, and there is no H contribution, $\lambda_H = \lambda_{hH} = 0$.

The parameters $f_q^{\mathcal{N}}$ in Eq. (18) depend on the so-called pion-nucleon sigma term $\sigma_{\pi N}$, which is not yet well-determined. To minimize the prediction for $\sigma_{\text{el}}^{\mathcal{N}}$ in view of the stringent experimental restraints, we estimate $f_q^{\mathcal{N}}$ using the results of Refs. [28, 29] with $\sigma_{\pi N} = 30$ MeV. This yields

$$\begin{aligned} f_u^p &= 0.01370, & f_d^p &= 0.01686, & f_s^p &= 0.06305, & f_{c,b,t}^p &= 0.06703, \\ f_u^n &= 0.00976, & f_d^n &= 0.02359, & f_s^n &= 0.06296, & f_{c,b,t}^n &= 0.06694. \end{aligned} \quad (\text{A10})$$

We note that $f_{c,b,t}^{\mathcal{N}} \simeq 2(1 - f_u^{\mathcal{N}} - f_d^{\mathcal{N}} - f_s^{\mathcal{N}})/27$.

Appendix B: Conditions for perturbativity, vacuum stability, and tree-level unitarity

The parameters of the scalar potential $\mathcal{V} = \mathcal{V}_H + \mathcal{V}_D$ of the THDM II+D in Eq. (8) are subject to a number of theoretical constraints. We adopt the usual assumption that the scalar interactions are in the perturbative regime, implying that the λ parameters in \mathcal{V} need to be capped. Thus, we demand that $|\lambda_{1,2,3,4,5}| \leq 8\pi$, like in the THDM scenario without the darkon [48], while for the darkon couplings $|\lambda_{D,1D,2D}| \leq 4\pi$ in view of their normalization convention in \mathcal{V} . In what follows, we describe additional requirements which may lead to stronger restraints on these λ s.

The requisite stability of \mathcal{V} implies that it has to be bounded from below. In other words, its quartic part

$$\begin{aligned} \mathcal{V}_4 &= \frac{1}{2}\lambda_1 (H_1^\dagger H_1)^2 + \frac{1}{2}\lambda_2 (H_2^\dagger H_2)^2 + \lambda_3 H_1^\dagger H_1 H_2^\dagger H_2 + \lambda_4 H_1^\dagger H_2 H_2^\dagger H_1 + \frac{1}{2}\lambda_5 \left[(H_1^\dagger H_2)^2 + \text{H.c.} \right] \\ &+ \frac{1}{4}\lambda_D D^4 + (\lambda_{1D} H_1^\dagger H_1 + \lambda_{2D} H_2^\dagger H_2) D^2 \end{aligned} \quad (\text{B1})$$

must stay positive for arbitrarily large values of the fields. Expressing

$$H_r^\dagger H_r = \eta_r^2, \quad \eta_r \geq 0, \quad r = 1, 2, \quad H_1^\dagger H_2 = \eta_1 \eta_2 \rho^2 e^{i\theta}, \quad 0 \leq \rho^2 \leq 1, \quad \text{Im } \theta = 0, \quad (\text{B2})$$

we then have

$$\begin{aligned} \mathcal{V}_4 &= \frac{1}{2} \begin{pmatrix} \eta_1^2 & \eta_2^2 & D^2 \end{pmatrix} \mathcal{M}_4 \begin{pmatrix} \eta_1^2 \\ \eta_2^2 \\ D^2 \end{pmatrix}, \\ \mathcal{M}_4 &= \begin{pmatrix} \lambda_1 & \lambda_3 + [\lambda_4 + \lambda_5 \cos(2\theta)]\rho^2 & \lambda_{1D} \\ \lambda_3 + [\lambda_4 + \lambda_5 \cos(2\theta)]\rho^2 & \lambda_2 & \lambda_{2D} \\ \lambda_{1D} & \lambda_{2D} & \frac{1}{2}\lambda_D \end{pmatrix}. \end{aligned} \quad (\text{B3})$$

For any of $\eta_{1,2}$ and D being large, $\mathcal{V}_4 > 0$ if \mathcal{M}_4 is strictly copositive [51], and this entails

$$\begin{aligned} \lambda_r &> 0, \quad \lambda_D > 0, \quad \lambda_{rD} > -\sqrt{\frac{1}{2}\lambda_r \lambda_D}, \quad \lambda_3 + \min(0, \lambda_4 - |\lambda_5|) > -\sqrt{\lambda_1 \lambda_2}, \\ 0 &< \lambda_{1D} \sqrt{2\lambda_2} + \lambda_{2D} \sqrt{2\lambda_1} + \left[\sqrt{\lambda_1 \lambda_2} + \lambda_3 + \min(0, \lambda_4 - |\lambda_5|) \right] \sqrt{\lambda_D} \\ &+ \sqrt{\left(\sqrt{2\lambda_1 \lambda_D} + 2\lambda_{1D} \right) \left(\sqrt{2\lambda_2 \lambda_D} + 2\lambda_{2D} \right) \left[\sqrt{\lambda_1 \lambda_2} + \lambda_3 + \min(0, \lambda_4 - |\lambda_5|) \right]}, \end{aligned} \quad (\text{B4})$$

where $r = 1, 2$.

Another important limitation is that the amplitudes for scalar-scalar scattering $s_1 s_2 \rightarrow s_3 s_4$ at high energies respect unitarity. Similarly to the THDM case [38, 49, 50], for the scalar pair $s_m s_n$ we can work with the nonphysical fields h_r^\pm , h_r^0 , and I_r^0 , as well as D . Accordingly, one can take the uncoupled sets of orthonormal pairs

$$\begin{aligned} & \{h_1^+ h_2^-, h_1^- h_2^+, h_1^0 h_2^0, h_1^0 I_2^0, I_1^0 h_2^0, I_1^0 I_2^0\}, \quad \{h_1^+ h_2^0, h_1^+ I_2^0, h_2^+ h_1^0, h_2^+ I_1^0\}, \\ & \left\{h_1^+ h_1^-, h_2^+ h_2^-, \frac{1}{\sqrt{2}} h_1^0 h_1^0, \frac{1}{\sqrt{2}} h_2^0 h_2^0, \frac{1}{\sqrt{2}} I_1^0 I_1^0, \frac{1}{\sqrt{2}} I_2^0 I_2^0, \frac{1}{\sqrt{2}} D D\right\}, \quad \{h_1^0 D, h_2^0 D\} \end{aligned} \quad (\text{B5})$$

to construct the matrix containing the tree-level amplitudes for $s_1 s_2 \rightarrow s_3 s_4$, which at high energies are dominated by the contributions of the four-particle contact diagrams. We can write the distinct eigenvalues of this matrix as

$$\begin{aligned} b_\pm &= \frac{1}{2}(\lambda_1 + \lambda_2) \pm \sqrt{\frac{1}{4}(\lambda_1 - \lambda_2)^2 + \lambda_4^2}, & c_\pm &= \frac{1}{2}(\lambda_1 + \lambda_2) \pm \sqrt{\frac{1}{4}(\lambda_1 - \lambda_2)^2 + \lambda_5^2}, \\ \mathbf{E}_\pm &= \lambda_3 + 2\lambda_4 \pm 3\lambda_5, & \mathbf{F}_\pm &= \lambda_3 \pm \lambda_4, & \mathbf{G}_\pm &= \lambda_3 \pm \lambda_5, & d_r &= 2\lambda_{rD}, \quad r = 1, 2, \end{aligned} \quad (\text{B6})$$

and the 3 solutions $a_{1,2,3}$ of the cubic polynomial equation

$$\begin{aligned} 0 &= a^3 - 3(\lambda_1 + \lambda_2 + \lambda_D)a^2 + [9\lambda_1\lambda_2 - (2\lambda_3 + \lambda_4)^2 + 9(\lambda_1 + \lambda_2)\lambda_D - 4\lambda_{1D}^2 - 4\lambda_{2D}^2]a \\ &+ 4[3\lambda_1\lambda_{2D}^2 + 3\lambda_2\lambda_{1D}^2 - 2(2\lambda_3 + \lambda_4)\lambda_{1D}\lambda_{2D}] + 3[(2\lambda_3 + \lambda_4)^2 - 9\lambda_1\lambda_2]\lambda_D. \end{aligned} \quad (\text{B7})$$

These results are consistent with those of Ref. [31]. The unitarity requirement for the $s_1 s_2 \rightarrow s_3 s_4$ amplitudes then translates into the constraints

$$|a_{1,2,3}|, |b_\pm|, |c_\pm|, |d_{1,2}|, |\mathbf{E}_\pm|, |\mathbf{F}_\pm|, |\mathbf{G}_\pm| \leq 8\pi. \quad (\text{B8})$$

The analogous conditions in the SM+D can be deduced from the foregoing by taking the one-Higgs-doublet limit. Thus, in the SM+D perturbativity demands $|\lambda_{\bar{H}}| \leq 8\pi$ for the Higgs self-coupling, $|\lambda_D| \leq 4\pi$, and $|\lambda| \leq 4\pi$, whereas from Eq. (B4) we have

$$\lambda_D > 0, \quad \lambda_{\bar{H}} > 0, \quad \lambda > -\sqrt{\frac{1}{2}\lambda_D\lambda_{\bar{H}}} \quad (\text{B9})$$

and from Eq. (B8)

$$\left| \frac{3}{2}(\lambda_D + \lambda_{\bar{H}}) \pm \sqrt{\frac{9}{4}(\lambda_D - \lambda_{\bar{H}})^2 + 4\lambda^2} \right| \leq 8\pi, \quad |\lambda_{\bar{H}}| \leq 8\pi, \quad |\lambda| \leq 4\pi. \quad (\text{B10})$$

The first inequalities in the last line imply the stronger caps $\lambda_{\bar{H}} \leq 8\pi/3$ and $\lambda_D \leq 8\pi/3$. The values of $|\lambda|$ shown in Fig. 2(a) are consistent with its limit in Eq. (B10).

To implement the conditions in Eqs. (B4) and (B8), we employ the relations

$$\begin{aligned} \lambda_1 &= \frac{s_\alpha^2 m_h^2 + c_\alpha^2 m_H^2}{c_\beta^2 v^2} - \frac{s_\beta m_{12}^2}{c_\beta^3 v^2}, & \lambda_2 &= \frac{c_\alpha^2 m_h^2 + s_\alpha^2 m_H^2}{s_\beta^2 v^2} - \frac{c_\beta m_{12}^2}{s_\beta^3 v^2}, \\ \lambda_3 &= \frac{s_{2\alpha}}{s_{2\beta}} \frac{m_H^2 - m_h^2}{v^2} + \frac{2m_{H^\pm}^2}{v^2} - \frac{2m_{12}^2}{s_{2\beta} v^2}, & \lambda_4 &= \frac{m_A^2 - 2m_{H^\pm}^2}{v^2} + \frac{2m_{12}^2}{s_{2\beta} v^2}, \\ \lambda_5 &= \frac{2m_{12}^2}{s_{2\beta} v^2} - \frac{m_A^2}{v^2}, & \lambda_{1D} &= \frac{c_\alpha \lambda_H - s_\alpha \lambda_h}{c_\beta}, & \lambda_{2D} &= \frac{c_\alpha \lambda_h + s_\alpha \lambda_H}{s_\beta}, \end{aligned} \quad (\text{B11})$$

derived from $\mathcal{V}_{H,D}$. Once α and β have been specified, $m_{h,H,A,H^\pm,12}$ and $\lambda_{h,H}$ can then serve as the free parameters instead of $\lambda_{1,2,3,4,5,1D,2D}$, as in Eqs. (13) and (A8). The expressions for $\lambda_{1,2,3,4,5}$ in Eq.(B11) agree with those in the literature [52].

-
- [1] K.A. Olive *et al.* [Particle Data Group Collaboration], Chin. Phys. C **38**, 090001 (2014) and 2015 update.
 - [2] D.S. Akerib *et al.*, arXiv:1608.07648 [astro-ph.CO].
 - [3] A. Tan *et al.* [PandaX-II Collaboration], Phys. Rev. Lett. **117**, no. 12, 121303 (2016) [arXiv:1607.07400 [hep-ex]].
 - [4] R. Bernabei *et al.*, Eur. Phys. J. C **73**, 2648 (2013) [arXiv:1308.5109 [astro-ph.GA]].
 - [5] R. Agnese *et al.* [CDMS Collaboration], Phys. Rev. Lett. **111**, no. 25, 251301 (2013) [arXiv:1304.4279 [hep-ex]].
 - [6] C.E. Aalseth *et al.* [CoGeNT Collaboration], Phys. Rev. D **88**, 012002 (2013) [arXiv:1208.5737 [astro-ph.CO]].
 - [7] G. Angloher *et al.*, Eur. Phys. J. C **72**, 1971 (2012) [arXiv:1109.0702 [astro-ph.CO]].
 - [8] J.H. Davis, C. McCabe, and C. Boehm, JCAP **1408**, 014 (2014) [arXiv:1405.0495]; G. Angloher *et al.* [CRESST-II Collaboration], Eur. Phys. J. C **74**, no. 12, 3184 (2014) [arXiv:1407.3146]; J.H. Davis, Int. J. Mod. Phys. A **30**, no. 15, 1530038 (2015) [arXiv:1506.03924].
 - [9] R. Agnese *et al.* [SuperCDMS Collaboration], Phys. Rev. Lett. **112**, no. 24, 241302 (2014) [arXiv:1402.7137 [hep-ex]].
 - [10] R. Agnese *et al.* [SuperCDMS Collaboration], Phys. Rev. Lett. **116**, no. 7, 071301 (2016) [arXiv:1509.02448 [astro-ph.CO]].
 - [11] G. Angloher *et al.* [CRESST Collaboration], Eur. Phys. J. C **76**, no. 1, 25 (2016) [arXiv:1509.01515 [astro-ph.CO]].
 - [12] P. Cushman *et al.*, arXiv:1310.8327 [hep-ex].
 - [13] E. Aprile *et al.* [XENON Collaboration], JCAP **1604**, no. 04, 027 (2016) [arXiv:1512.07501 [physics.ins-det]].
 - [14] C.E. Aalseth *et al.*, Adv. High Energy Phys. **2015**, 541362 (2015). doi:10.1155/2015/541362
 - [15] D.S. Akerib *et al.* [LZ Collaboration], arXiv:1509.02910 [physics.ins-det].
 - [16] J. Billard, L. Strigari, and E. Figueroa-Feliciano, Phys. Rev. D **89**, no. 2, 023524 (2014) [arXiv:1307.5458 [hep-ph]].
 - [17] A. Kurylov and M. Kamionkowski, Phys. Rev. D **69**, 063503 (2004) [arXiv:hep-ph/0307185]; F. Giuliani, Phys. Rev. Lett. **95**, 101301 (2005) [arXiv:hep-ph/0504157].
 - [18] J.L. Feng, J. Kumar, D. Marfatia, and D. Sanford, Phys. Lett. B **703**, 124 (2011) [arXiv:1102.4331].
 - [19] J.L. Feng, J. Kumar, and D. Sanford, Phys. Rev. D **88**, no. 1, 015021 (2013) [arXiv:1306.2315].
 - [20] C. Savage, G. Gelmini, P. Gondolo, and K. Freese, JCAP **0904**, 010 (2009) [arXiv:0808.3607].
 - [21] N. Chen, Q. Wang, W. Zhao, S.T. Lin, Q. Yue, and J. Li, Phys. Lett. B **743**, 205 (2015) [arXiv:1404.6043]; C.Q. Geng, D. Huang, C.H. Lee, and Q. Wang, JCAP **1608**, no. 08, 009 (2016) [arXiv:1605.05098 [hep-ph]].
 - [22] S. Scopel and K.H. Yoon, JCAP **1602**, no. 02, 050 (2016) [arXiv:1512.00593 [astro-ph.CO]].
 - [23] V. Silveira and A. Zee, Phys. Lett. B **161**, 136 (1985).
 - [24] C.P. Burgess, M. Pospelov, and T. ter Veldhuis, Nucl. Phys. B **619**, 709 (2001) [arXiv:hep-ph/0011335]; M.C. Bento *et al.*, Phys. Rev. D **62**, 041302 (2000) [astro-ph/0003350];

- M.C. Bento, O. Bertolami, and R. Rosenfeld, Phys. Lett. B **518**, 276 (2001) [hep-ph/0103340]; D.E. Holz and A. Zee, Phys. Lett. B **517**, 239 (2001) [hep-ph/0105284]; H. Davoudiasl *et al.*, Phys. Lett. B **609**, 117 (2005) [arXiv:hep-ph/0405097]; V. Barger *et al.*, Phys. Rev. D **77**, 035005 (2008) [arXiv:0706.4311]; S. Andreas, T. Hambye, and M.H.G. Tytgat, JCAP **0810**, 034 (2008) [arXiv:0808.0255]; C.E. Yaguna, JCAP **0903**, 003 (2009) [arXiv:0810.4267]; M. Gonderinger *et al.*, JHEP **1001**, 053 (2010) [arXiv:0910.3167]; X.G. He *et al.*, Phys. Lett. B **688**, 332 (2010) [arXiv:0912.4722]; M. Asano and R. Kitano, Phys. Rev. D **81**, 054506 (2010) [arXiv:1001.0486]; S. Andreas *et al.*, Phys. Rev. D **82**, 043522 (2010) [arXiv:1003.2595]; A. Badin and A.A. Petrov, Phys. Rev. D **82**, 034005 (2010) [arXiv:1005.1277]; W.L. Guo and Y.L. Wu, JHEP **1010**, 083 (2010) [arXiv:1006.2518]; Nucl. Phys. B **867**, 149 (2013) [arXiv:1103.5606]; S. Profumo, L. Ubaldi, and C. Wainwright, Phys. Rev. D **82**, 123514 (2010) [arXiv:1009.5377]; A. Abada, D. Ghaffor, and S. Nasri, Phys. Rev. D **83**, 095021 (2011) [arXiv:1101.0365]; G. Cynolter, E. Lendvai, and G. Pocsik, Acta Phys. Polon. B **36**, 827 (2005) [hep-ph/0410102]; A. Biswas and D. Majumdar, Pramana **80**, 539 (2013) [arXiv:1102.3024]; K. Ghosh *et al.*, Phys. Rev. D **84**, 015017 (2011) [arXiv:1105.5837]; Y. Mambrini, Phys. Rev. D **84**, 115017 (2011) [arXiv:1108.0671]; M. Raidal and A. Strumia, Phys. Rev. D **84**, 077701 (2011) [arXiv:1108.4903]; I. Low *et al.*, Phys. Rev. D **85**, 015009 (2012) [arXiv:1110.4405]; O. Lebedev, H.M. Lee, and Y. Mambrini, Phys. Lett. B **707**, 570 (2012) [arXiv:1111.4482]; A. Drozd, B. Grzadkowski, and J. Wudka, JHEP **1204**, 006 (2012) [*Erratum ibid.* **1411**, 130 (2014)] [arXiv:1112.2582]; A. Djouadi *et al.*, Phys. Lett. B **709**, 65 (2012) [arXiv:1112.3299]; Y. Mambrini *et al.*, JCAP **1211**, 038 (2012) [arXiv:1206.2352]; K. Cheung *et al.*, JCAP **1210**, 042 (2012) [arXiv:1207.4930]; L.B. Jia and X. Q. Li, Phys. Rev. D **89**, no. 3, 035006 (2014) [arXiv:1309.6029]; F.S. Queiroz, K. Sinha, and A. Strumia, Phys. Rev. D **91**, no. 3, 035006 (2015) [arXiv:1409.6301]; L. Feng, S. Profumo, and L. Ubaldi, JHEP **1503**, 045 (2015) [arXiv:1412.1105]; M. Duerr, Phys. Lett. B **751**, 119 (2015) [arXiv:1508.04418]; JHEP **1606**, 152 (2016) [arXiv:1509.04282]; JHEP **1606**, 008 (2016) [arXiv:1510.07562]; H. Han and S. Zheng, JHEP **1512**, 044 (2015) [arXiv:1509.01765]; H. Han *et al.*, Phys. Lett. B **756**, 109 (2016) [arXiv:1601.06232]; F.S. Sage and R. Dick, arXiv:1604.04589 [astro-ph.HE].
- [25] J.M. Cline *et al.*, Phys. Rev. D **88**, 055025 (2013); **92**, no. 3, 039906(E) (2015) [arXiv:1306.4710].
- [26] J. McDonald, Phys. Rev. D **50**, 3637 (1994) [arXiv:hep-ph/0702143]; V. Barger, M. McCaskey, and G. Shaughnessy, Phys. Rev. D **82**, 035019 (2010) [arXiv:1005.3328]; J.K. Mizukoshi *et al.*, Phys. Rev. D **83**, 065024 (2011) [arXiv:1010.4097]; M. Gonderinger, H. Lim, and M.J. Ramsey-Musolf, Phys. Rev. D **86**, 043511 (2012) [arXiv:1202.1316]; C.W. Chiang, T. Nomura, and J. Tandean, Phys. Rev. D **87**, no. 7, 073004 (2013) [arXiv:1205.6416]; R. Coimbra, M.O.P. Sampaio, and R. Santos, Eur. Phys. J. C **73**, 2428 (2013) [arXiv:1301.2599]; S. Baek, P. Ko, and W.I. Park, Phys. Rev. D **90**, no. 5, 055014 (2014) [arXiv:1405.3530]; R. Costa *et al.*, Phys. Rev. D **92**, 025024 (2015) [arXiv:1411.4048]; R. Costa *et al.*, JHEP **1606**, 034 (2016) [arXiv:1512.05355].
- [27] C. Bird, R. Kowalewski, and M. Pospelov, Mod. Phys. Lett. A **21**, 457 (2006) [arXiv:hep-ph/0601090]; X.G. He *et al.*, Mod. Phys. Lett. A **22**, 2121 (2007) [arXiv:hep-ph/0701156].
- [28] X.G. He, B. Ren, and J. Tandean, Phys. Rev. D **85**, 093019 (2012) [arXiv:1112.6364 [hep-ph]]; X.G. He and J. Tandean, Phys. Rev. D **88**, 013020 (2013) [arXiv:1304.6058 [hep-ph]].
- [29] X.G. He *et al.*, Phys. Rev. D **79**, 023521 (2009) [arXiv:0811.0658 [hep-ph]].
- [30] B. Grzadkowski and P. Osland, Phys. Rev. D **82**, 125026 (2010) [arXiv:0910.4068]; M. Aoki, S. Kanemura, and O. Seto, Phys. Lett. B **685**, 313 (2010) [arXiv:0912.5536]; T. Li and Q. Shafi, Phys. Rev. D **83**, 095017 (2011) [arXiv:1101.3576]; Y. Cai, X.G. He, and B. Ren, Phys. Rev. D **83**, 083524 (2011) [arXiv:1102.1522]; Y. Bai *et al.*, Phys. Rev. D **88**, 015008 (2013) [arXiv:1212.5604];

- Y. Cai and T. Li, Phys. Rev. D **88**, no. 11, 115004 (2013) [arXiv:1308.5346]; A. Greljo *et al.*, JHEP **1311**, 190 (2013) [arXiv:1309.3561]; L. Wang and X.F. Han, Phys. Lett. B **739**, 416 (2014) [arXiv:1406.3598]; N. Okada and O. Seto, Phys. Rev. D **90**, no. 8, 083523 (2014) [arXiv:1408.2583]; R. Campbell *et al.*, Phys. Rev. D **92**, no. 5, 055031 (2015) [arXiv:1505.01793]; A. Drozd *et al.*, JCAP **1610**, no. 10, 040 (2016) [arXiv:1510.07053].
- [31] A. Drozd *et al.*, JHEP **1411**, 105 (2014) [arXiv:1408.2106];
- [32] G. Aad *et al.* [ATLAS and CMS Collaborations], Phys. Rev. Lett. **114**, 191803 (2015) [arXiv:1503.07589 [hep-ex]].
- [33] S. Heinemeyer *et al.* [LHC Higgs Cross Section Working Group Collaboration], arXiv:1307.1347 [hep-ph]. Online updates available at <https://twiki.cern.ch/twiki/bin/view/LHCPhysics/CERNYellowReportPageBR2014>.
- [34] The ATLAS and CMS Collaborations, JHEP **1608**, 045 (2016) [arXiv:1606.02266 [hep-ex]].
- [35] X.G. He, S.Y. Ho, J. Tandean, and H.C. Tsai, Phys. Rev. D **82**, 035016 (2010) [arXiv:1004.3464 [hep-ph]]; X.G. He and J. Tandean, Phys. Rev. D **84**, 075018 (2011) [arXiv:1109.1277 [hep-ph]].
- [36] H.Y. Cheng and C.W. Chiang, JHEP **1207**, 009 (2012) [arXiv:1202.1292 [hep-ph]].
- [37] J.F. Gunion, H.E. Haber, G.L. Kane, and S. Dawson, *The Higgs Hunter's Guide* (Westview Press, Colorado, 2000).
- [38] For a recent review, see G.C. Branco, P.M. Ferreira, L. Lavoura, M.N. Rebelo, M. Sher, and J.P. Silva, Phys. Rept. **516**, 1 (2012) [arXiv:1106.0034 [hep-ph]].
- [39] M.A. Shifman, A.I. Vainshtein, and V.I. Zakharov, Phys. Lett. B **78**, 443 (1978); T.P. Cheng, Phys. Rev. D **38**, 2869 (1988); H.Y. Cheng, Phys. Lett. B **219**, 347 (1989).
- [40] J. Meija *et al.*, Pure Appl. Chem. **88**, no. 3, 293 (2016).
- [41] C.S. Chen, C.Q. Geng, D. Huang, and L.H. Tsai, Phys. Rev. D **87**, 075019 (2013) [arXiv:1301.4694].
- [42] M.E. Peskin and T. Takeuchi, Phys. Rev. D **46**, 381 (1992).
- [43] W. Grimus, L. Lavoura, O.M. Ogreid, and P. Osland, Nucl. Phys. B **801**, 81 (2008) [arXiv:0802.4353].
- [44] P. Gondolo and G. Gelmini, Nucl. Phys. B **360**, 145 (1991).
- [45] E.W. Kolb and M. Turner, *The Early Universe* (Westview Press, Boulder, 1990).
- [46] G. Steigman, B. Dasgupta, and J.F. Beacom, Phys. Rev. D **86**, 023506 (2012) [arXiv:1204.3622].
- [47] P.A.R. Ade *et al.* [Planck Collaboration], Astron. Astrophys. **594**, A13 (2016) [arXiv:1502.01589 [astro-ph.CO]].
- [48] S. Kanemura, T. Kasai, and Y. Okada, Phys. Lett. B **471**, 182 (1999) [hep-ph/9903289].
- [49] S. Kanemura, T. Kubota, and E. Takasugi, Phys. Lett. B **313**, 155 (1993) [hep-ph/9303263].
- [50] A.G. Akeroyd, A. Arhrib, and E.M. Naimi, Phys. Lett. B **490**, 119 (2000) [hep-ph/0006035].
- [51] K. Hadeler, Linear Algebra Appl. **49**, 79 (1983); G. Chang and T.W. Sederberg, Comput. Aided Geom. Des. **11** (1), 113 (1994); L. Ping and F.Y. Yu, Linear Algebra Appl. **194**, 109 (1993); K. Kannike, Eur. Phys. J. C **72**, 2093 (2012) [arXiv:1205.3781 [hep-ph]].
- [52] J.F. Gunion and H.E. Haber, Phys. Rev. D **67**, 075019 (2003) [hep-ph/0207010].